Svep1 stabilizes developmental vascular anastomosis in reduced flow conditions

Baptiste Coxam[1,2], Russell T. Collins[1,2], Melina Hußmann[3], Yvonne Huisman[3], Katja Meier[1], Simone Jung[1], Eireen Bartels-Klein[1], Anna Szymborska[1], Lise Finotto[5,6], Christian S.M. Helker[7,8], Didier Y.R. Stainier[7], Stefan Schulte-Merker[3], Holger Gerhardt[1,2,4]

1 - Integrative Vascular Biology Lab, Max-Delbrück Center for Molecular Medicine in the Helmholtz Association (MDC), Robert-Rössle-Strasse 10, Berlin 13125, Germany

2 - DZHK (German Center for Cardiovascular Research), partner site Berlin

3 – Institute of Cardiovascular Organogenesis and Regeneration, Faculty of Medicine, WWU Münster, Mendelstraße 7, 48149 Münster, Germany

4 - Berlin Institute of Health (BIH), Berlin, Germany

5 – Vascular Patterning Laboratory, Center for Cancer Biology, VIB, Leuven, Belgium

6 – Vascular Patterning Laboratory, Department of Oncology, KU Leuven, Leuven, Belgium

7 – Department of Developmental Genetics, Max Planck Institute for Heart and Lung Research, Bad Nauheim, 61231, Germany

8 – Current address: Philipps-University Marburg, Faculty of Biology, Cell Signaling and Dynamics, Marburg, 35043, Germany

corresponding author: Prof. Dr. Holger Gerhardt

Integrative Vascular Biology

BIH and DZHK professorship for Experimental Cardiovascular Research at the Charité

Robert-Rössle-Straße 10, 13125 Berlin, Germany

Phone: +49 (0)30 9406-1780

Fax: +49 (0)30 9406-1771

holger.gerhardt@mdc-berlin.de

Abstract

Molecular mechanisms controlling the formation, stabilization and maintenance of blood vessel connections remain poorly defined. Here we identify blood flow and the large extracellular protein Svep1 as co-modulators of vessel anastomosis during developmental angiogenesis in zebrafish embryos. Both loss of Svep1 and blood flow reduction contribute to defective anastomosis of intersegmental vessels. The reduced formation and lumenisation of the dorsal longitudinal anastomotic vessel (DLAV) is associated with a compensatory increase in Vegfa/Vegfr pERK signalling, concomittant expansion of *apelin*-positive tip cells, but reduced expression of *klf2*. Experimentally, further increasing Vegfa/Vegfr signalling can rescue the DLAV formation and lumenisation defects, while its inhibition dramatically exacerbates the loss of connectivity. Mechanistically, our results suggest that flow and Svep1 co-regulate the stabilization of vascular connections, in part by modulating the Vegfa/Vegfr signalling pathway.

Non-standards Abbreviations and Acronyms

DLAV: dorsal longitudinal anastomotic vessel

hpf: hours post-fertilization

ISVs: intersegmental vessels

DA: Dorsal Aorta

PCV: Posterior Cardinal Vein

VEGFR-2: vascular endothelial growth factor receptor-2

Kdr; Kinase insert domain receptor

Kdrl: Kinase insert domain receptor like

VEGFA: vascular endothelial growth factor A

MO: Morpholino

Introduction

Angiogenesis defines the formation of new vessels from pre-existing ones and is a stepwise process that leads to the establishment of a perfused network of arteries and veins that are optimally organised to serve the metabolic needs of the developing embryo. In zebrafish embryos, the initial coalescence of endothelial progenitor cells in a process termed vasculogenesis shapes the two main axial blood vessels, namely the dorsal aorta (DA) and the posterior cardinal vein (PCV). Later, angiogenic sprouts emerge from the DA. These multicellular sprouts are composed of a leading tip cell followed by stalk cells [1], and migrate dorsally in between vertical somite boundaries to form the intersegmental vessels (ISVs)[2]. The proliferation of endothelial cells in ISVs and their migration to the dorsal part of the embryo is driven by Vegfa signalling, through binding to the zebrafish VEGFR2 ortholog Kdr and its

ohnolog Kdrl [3-8] . Activation of Kdrl signalling in the leading ISV endothelial cell (tip), mediated in large part via the phosphorylation of the serine/threonine kinase ERK1/2, promotes migratory behaviour. In parallel, activation of Kdrl signalling in the tip cell leads to Notch mediated inhibition of Kdrl signalling in trailing cells (stalks), preventing their conversion into tip cells and promoting their proliferation to support ISV expansion [6, 9, 10]. Around 30-32 hours post-fertilisation (hpf), the leading tip cells of the ISVs start to anastomose with their ipsilateral neighbours, a process that ultimately leads to the formation of the dorsal longitudinal anastomotic vessel (DLAV), dorsal to the neural tube [11, 12]. The DLAV is initially a paired bilateral structure that is fully lumenised by 48 hpf, but subsequently both sides progressively connect to form a complex plexus [2, 12]. Zygmunt and colleagues [12] demonstrated that maturation of the DLAV plexus is regulated by flow and Vegfr signalling after 48 hpf. However, while they show that flow is dispensable for the initial formation of the DLAV, little is known about the cellular mechanism driving the anastomosis of ipsilateral ISVs and the lumenisation of the DLAV segments during DLAV formation (32 to 48 hpf).

Recent reports have characterised the importance of Svep1/Polydom, a secreted extracellular matrix (ECM) protein that can mediate cell to substrate adhesion in-vitro in an integrin $\alpha 9\beta 1$-dependent manner [13], as a regulator of secondary angiogenesis [14, 15]. In zebrafish, loss-of-function *svep1* mutants exhibit a reduced number of venous and lymphatic precursors (parachordal lymphangioblasts, PLs) emerging from the PCV during secondary angiogenesis (from 32 hpf). In addition, PLs show reduced migration from the horizontal myoseptum. Both these defects lead to an increased number of arterial ISVs (aISVs) and a severe reduction in the lymphatic trunk vasculature. Here, we uncover a novel and distinct role for Svep1 in

the regulation of DLAV formation under reduced flow conditions, acting in part through the modulation of Vegfa/Vegfr signalling in endothelial cells.

Material and Methods

Zebrafish husbandry and transgenic lines

Zebrafish (*Danio rerio*) were raised and staged as previously described [16]. The following transgenic lines were used: *Tg[fli1a:EGFP]*^{y1} [17] (labels all endothelial cells), *Tg[gata1a:dsRed]*^{sd2} [18] (label all erythrocytes), *Tg[-0.8flt1:RFP]*^{hu5333} [5] (strongly labels arterial endothelial cells), *TgBAC(apln:eGFP)*^{bns157} *[19] (labels endothelial tip cells)*,*TgBAC[svep1:GAL4FF]*^{hu8885}*;Tg(5xUAS:EGFP)*^{nkuasgfp1a} *Tg(svep1:Gal4FF;UAS:GFP)* (labels *svep1* positive cells) [14]. The *svep*^{hu4767} mutant line has been described previously [14]. For growing and breeding of transgenic lines we comply with regulations of the ethical commission animal science of MDC Berlin and with FELASA guidelines [20].

Tricaine treatment

To slow down heart rate and blood flow during DLAV formation, embryos were treated with 0.007%, 0.014% (1X) or 0.028% (2X) tricaine (MS-222, Sigma) between 30 and 48 hpf, as indicated in the figure legends.

Morpholino knockdown

Morpholinos against *svep1* (5ng), *flt1* (1ng), *gata1* (8ng) and *tnnt2* (4ng) were used as previously described [12, 15, 21, 22] and injected in the yolk of zebrafish embryos at the one-cell stage.

mRNA injections

To generate mRNA for injections, pmtb-t7-alpha-bungarotoxin (gift from Sean Megason) (Addgene plasmid # 69542 ; http://n2t.net/addgene:69542 ; RRID:Addgene_69542) [23] was digested with EcoRV and mRNA transcribed using HiScribe T7 ARCA mRNA Kit (New England Biolabs). Control mRNA (GFP) was translated from XbaI digested pCS2+EGFP using the mMESSAGE mMACHINE SP6 Transcription kit (Invitrogen). 50pg of mRNA was injected into 1-2 cell stage embryos as described.

In situ hybridization

A synthetic, double stranded DNA fragment (Eurofins) with the complete coding sequence from Danio rerio *klf2a* mRNA (Genbank accession number: NM_131856) was inserted into EcoRV digested pISceI using NEBuilder HiFi DNA Assembly (New England Biolabs). The plasmid was digested with BamHI (anti-sense) or XhoI (sense) and probes transcribed using 20 U/µl T7 (anti-sense) or Sp6 (sense) polymerase (Promega) with digoxigenin labelling mix. 48 hpf embryos were treated with 0.02 mg/µl Proteinase K for 30 min. The *in situ* hybridizations were performed as previously described[24, 25]. Embryos were dehydrated in methanol and mounted in glycerol for imaging. In situ hybridization with sense probe occasionally resulted in weak diffuse background staining (not shown).

Statistical Analysis

All quantifications were performed in the trunk region of zebrafish embryos, across 7-9 somites. (N) refers to experiments, (n) refers to embryos. Statistical analysis was performed with Mann-Whitney-U tests, unless indicated otherwise. No statistical method was used to predetermine sample size. Data represent mean ± STDEV of

representative experiments (except when indicated otherwise). Statistical tests were conducted using Prism (GraphPad) software. Adequate tests were chosen according to the data to fulfil test assumptions. Sample sizes, number of repeat experiments, performed tests and p-values are indicated per experiment.

Zebrafish embryos were selected based on the following pre-established criteria: normal morphology, beating heart, presence of circulating red blood cells. The experiments were not randomized. For every experiment treated and control embryos were derived from the same egg lay. The investigators were not blinded to allocation during experiments and outcome assessment.

Live imaging

Embryos were anaesthetized in 0.014% tricaine (MS-222, Sigma), mounted in a 35 mm glass bottom petri dish (0.17 mm, MatTek) using 0.6-1% reduced melting point agarose (Sigma) containing 0,014% tricaine, and bathed in E3 media containing 0.014%(1X tricaine and 0.003% PTU). Time-lapse imaging was performed using an upright 3i spinning-disc confocal using a Zeiss Plan-Apochromat, 20x, 40x/1.0 NA water-dipping objective. Image processing was performed using Fiji software [26].

Isolation of endothelial cells

48 hpf *Tg[fli1a: nEGFP]*^{y7} and *Tg[fli1a: EGFP]*^{y1} crossed to *Tg[gata1:dsRed]* embryos were dechorionated using a solution of 1mg/mL Pronase (Sigma Aldrich) on an orbital shaker for 10 minutes at room temperatures. Up to 250 dechorionated embryos per conditions were anaesthetized with 1X (0.014%) tricaine and transferred to a 1.5 mL Eppendorf with 1 mL calcium-free Ringer solution (116 mM NaCL, 2.9 mM KCL, 5 mM HEPES pH7.2) to remove the yolks. After pipetting gently up and

down with a 1mL tip the embryos were centrifugated at 2000 rpm for 5 minutes at 4C. The supernatant was removed, and the procedure repeated until all the yolks were removed and the solution clear. The calcium-free ringer solution was replaced with 1 mL of protease solution (72 μg/mL Liberase DH research grade from Merck/Sigma, 0.4U/mL DNaseI-Invitrogen). The embryos were incubated at 28.5C on an orbital shaker for 20 minutes, pipetting up and down with a 200μL tip every 3 minutes, to form a homogenous solution of cells. The dissociation process was stopped by placing the embryos on ice and adding 2μL CaCl2 and 0.5 μL FBS per mL. The cell suspension was centrifuged at 2000 rpm for 5 minutes at 4C. The supernatant was discarded, and the cells resuspended in sorting solution (2mM EDTA, 0.4U/mL DNaseI, 0.5% FBS in DPBS). The solution was passed through a 40μm strainer inside a 50 mL falcon tube, previously washed with 500μL sorting solution. Following filtration, 500μL sorting solution was added to the strainer. The filtered solution was centrifuged at 2000 RPM for 5 minutes at 4°C. The supernatant was removed, and the cell resuspended in 700 μL sorting solution. The cell suspension was then loaded onto an ARIA III FACsorter (BD Bioscience). Using *Tg[gata1:dsRED]* only embryos for gating, we specifically sorted GFP+, dsRED- cells to remove red blood cells with active *fli1a* promoter activation at that developmental stage. The cells were then centrifuged, all the supernatant removed, and cells stored immediately at -80C until protein extraction.

Protein extraction

Sorted embryos were treated with 40μL Lysis Buffer (1mL 1M Tris-HCl, 0.4 mL 0.5M EDTA, 8.75 mL 10% Brij 96, 1.25 mL 10% NP-40 to 100mL with dH2O) and 0.4μL Protease Inhibitor cocktail (ThermoFischer). The samples were homogenized with a

pestle and centrifuged at 13000 RPM for 15 minutes at 4°C. The protein supernatant was collected, and protein concentration assessed using a BCA protein assay kit (ThermoFischer).

Western Blot

20-50μg of the protein lysates (equal amount for each condition to compare) diluted in 18.7μL water and 6.3μL loading buffer (25μL total volume) and heated for 5 min at 95°C to denaturise the proteins. The samples were loaded and run alongside a 10μl ladder marker (Novex Sharp Pre-Stained - thermoFischer) for 1h at 150V and subsequently transferred onto previously MeOH activated polyvinylidene fluoride membranes. Membranes were blocked with Blocking solution (5% nonfat dry milk in 50 mg/mL TBS-T) for 1.5h at room temperature and then incubated with primary antibody against p-ERK, overnight at 4°C (1:250, *(Erk1/2) (Thr202/Tyr204)* #9101, Cell Signaling Technology). After incubation with primary antibody, the membranes were washed 4 times in 50 mg/mL TBS-T and then incubated with secondary antibodies (1:4000 anti-rabbit) and washed 3 times with 50 mg/mLTBS-T. Immunodetection was performed using a chemiluminescence kit (1mL SuperSignal West Dura; Pierce), and bands were developed using the Las-4000 imaging system. After initial immunodetection, membranes were stripped of antibodies by using the Stripping kit (ThermoFisher) at 56°C for 40min and re-probed with anti–GFP antibody for 1h (1:1000, Origene R1091P). Band intensity was measured and using the histogram function on the Fiji software, with control and treated samples on the same blot [26].

Blood flow and heart rate measurements

Embryos were anaesthetized in 0.014% tricaine (MS-222, Sigma) from 30 to 48 hpf before being mounted in a petri dish using 1% low melting point agarose (Sigma) containing 0.014% (1X) tricaine, and bathed in Danieau's buffer containing (1X) tricaine respectively and 0.003% PTU, and imaged on an upright 3i spinning-disc confocal using a Zeiss Plan-Apochromat , 20x/1.0 NA water-dipping objective with a frame interval of 10ms. Kymographs were generated using the MultipleKymograph plugin in ImageJ to quantify heart rate over an 8 second period, synced to the beginning of a heartbeat (line width: 1).

To estimate instantaneous blood flow speed, we cropped images of the dorsal aorta and measured average frame-to-frame translation of red blood cells using the Kuglin-Hines algorithm (Kuglin and Hines, 1975) for image phase-correlation. In brief, the phase correlation map between two adjacent frames was calculated by multiplying the Fast Fourier transform (FFt) of $frame_i$ and a conjugate FFt of $frame_{i+1}$. The inverse FFt of the phase correlation gives a correlation map with a peak offset from the center by the relative shift between the frames. The position of the peak was determined by finding the local maximum in a Gaussian filtered correlation map. The velocity data was smoothed with a moving average filter with a span of 5 frames. Analysis was performed in Matlab (Mathworks, Inc.).

Chemical treatment

Where indicated, embryos were treated with VEGFR inhibitors ZM323881 (Tocris Bioscience) or SU5416 (sigma Aldrich), from 30 to 48hpf, in addition to 0.003% PTU and the indicated amount of tricaine.

Results

svep1 mutant and morphant zebrafish embryos exhibit vascular anastomosis defects.

While imaging angiogenesis in the trunk of *svep1*^{hu4767} loss-of-function mutants [14] from 30 to 48 hpf, we noticed that a significant number of primary angiogenic sprouts failed to anastomose with their ipsilateral neighbours (Figure 1A) (Supplementary Video 1, 2). In the majority of cases (74% ± 33), the DLAV gaps arise following the regression of a pre-existing connection between ipsilateral neighbouring ISVs, rather than an absence of connection (N=6 experiments, n=18 mutants). Additionally, only a minority of these connections (13%, N=6 experiments, n=17 mutants) were transiently lumenised before regressing. These results suggest that in this context, *svep1* loss-of-function negatively affects the stabilisation of vascular connections between neighbouring sprouts.

We quantified the number of gaps in the DLAV, and lumenisation status of existing DLAV segments at 48 hpf, a time at which the DLAV is considered fully formed and almost fully lumenised in wild-type (WT) zebrafish embryos [2, 12]. *svep1*^{hu4767} mutants exhibited a significantly increased number of gaps in their DLAV at 48 hpf (25.5% ± 23.4 versus 2.6% ± 5.6 in their WT siblings) and a significant decrease of lumenised DLAV segments (47.8 % ± 33.1 versus 86.4 % ± 17.3) (Figure 1B-D). These phenotypes were also observed in *svep1* morphants compared to control morphants (DLAV gaps: 36.3% ± 25.4 versus 6% ± 10.9; lumenised DLAV segments: 46.1% ± 33.8 versus 94.7 ± 10.5) (Figure 1E, F). In addition, while the expressivity of the morphant phenotype in different zebrafish transgenic lines varied markedly, we observed a statistically significant difference between *svep1* and control morphants in

all cases (Supplementary Figure 1A, B). Finally, we found a variable expressivity of the *svep1*^{hu4767} homozygous mutant DLAV phenotype between clutches (Supplementary Figure 1C-F).

svep1 loss-of-function sensitises angiogenic remodelling to reduced blood flow.

Surprisingly, we could not detect any anastomosis defects at the DLAV in *svep1*^{hu4767} mutants and morphants when imaged at 48 hpf, whilst they continued to exhibit the previously reported PL phenotypes [14] (PLs at the horizontal myoseptum: 47.6% ± 17.5 versus 80.2% ± 19.4% in WT clutch mates and aISVs: 65.4% ± 15.1 versus 49.3% ± 15 in WT siblings, N=4, n=12 mutants, n=25 WT)). The DLAV phenotypes instead only occurred in mutant embryos that were imaged live from 30 to 48 hpf. Upon closer inspection, we found that treatment with tricaine (tricaine mesylate – MS222), a muscle relaxant commonly used to immobilise zebrafish embryos, lead to a dose-dependent emergence of the DLAV phenotypes in *svep1* loss-of-function morphants (Figure 2A, B) following treatment with concentration of 1X (0.014%) or above from 30 to 48 hpf.

In addition, removal of tricaine from mutant embryos at 48 hpf led to a significant recovery of the DLAV vasculature at 72 hpf, with only 27% (± 26) of the DLAV gaps still present at that stage (supplementary Figure 2A, B).

Previous work has revealed that *svep1* loss-of-function is associated with cardiac defects [14]. To test if *svep1* loss-of-function further sensitises embryos to blood flow reduction, we quantified heartbeats per minutes in control and *svep1* morphants and found no differences in embryos treated with 1X (0.014%) or 2X (0.028%) tricaine

from 30 to 48 hpf (supplementary Figure 2C). However, we found that mean blood flow speed was significantly decreased in *svep1* morphants compared to control morphants when treated with 1X tricaine (MO-CTL 5ng: 679um/s ± 205, MO-svep1 5ng: 521 um/s ± 190). This suggest that the cardiac phenotype detected in *svep1* loss-of-function embryos exacerbates the blood flow reduction induced by tricaine treatment.

To further characterize the phenotype we decided to begin our investigation at 30 hpf, as this time point marks the beginning of ISV ipsilateral anastomosis in most embryos (Figure 1A). As tricaine treatment leads to a reduction of blood flow speed [27], we investigated whether a general blood flow speed reduction or a reduction of erythrocytes-dependent shear stress was responsible for the DLAV phenotype in *svep1* morphants. In the absence of tricaine treatment, joint inhibition of *svep1* function and erythrocyte formation, using *svep1* and *gata1* morpholinos, did not lead to any DLAV phenotypes (Figure 2C, D). However, in the absence of tricaine treatment, abolition of cardiac function, and thus blood flow, using a morpholino against *troponin T type 2a* (*tnnt2a*) led to a DLAV phenotype in *svep1* morphants (Figure 2E, F and G) (16.4% ± 16.2 versus 3.5 ± 6.2 in *svep1* morphants only). Abolition of blood flow in *svep1* homozygous mutants led to an increase in the proportion of fish exhibiting a strong DLAV phenotype (30% compared to 5.3% of WT clutch mate) (Supplementary Figure 2F). These results suggest that *svep1* loss-of-function has an additive effect in affecting blood vessels anastomosis when blood flow is reduced, and that *svep1* loss-of-function further sensitises primary ISVs anastomosis to reduced blood flow or pressure, but not reduced shear stress.

klf2a, a key transcription factor gene upregulated by laminar shear stress in endothelial cells[28], also showed reduced expression after tricaine treatment or *svep1* knockdown, and almost complete absence from ISVs when *svep1* knockdown was combined with tricaine (Figure 2H). In contrast to ISVs and DLAV, the major axial vessels showed no reduction in *klf2* expression, further suggesting that shear sensing in general is not affected by tricaine and/or *svep1* loss-of-function.

In addition, we observed that *svep1* loss-of-function significantly increases the percentage of short ISVs in *tnnt2a* morphants at 48 hpf (14.6% ± 10.5 versus 4.8% ± 7.6 in *tnnt2a* morphants only). This led us to investigate the importance of *svep1* in the regulation of angiogenic sprout identity and behaviour under reduced flow conditions.

Svep1 is expressed in neurons of the neural tube and its expression is flow dependent

Imaging of the *svep1* reporter line *Tg(svep1: Gal4FF;UAS:GFP)* [14] at 48 hpf showed strong GFP expression in dorsal epithelial cells above the neural tube, and in individual neurons of the neural tube (Figure 3A, Supplementary Figure 3A, B). Treatment with 1X tricaine from 30 to 48 hpf led to a significant reduction in *svep1* expression throughout the trunk area, particularly in the neural tube at 48 hpf (Figure 3B). In addition, tricaine treatment between 30 and 48 hpf lead to a significant reduction in endogenous *svep1* mRNA expression within the neural tube and ventral somite boundary (supplementary Figure 3C), suggesting that blood flow not only sensitises angiogenic sprouts to *svep1* downregulation, but also directly affects *svep1* expression.

Given that tricaine, in addition to lowering cardiac function, has additional effects on neural voltage-gated sodium channels [29], and that we observe reduced neural expression of *svep1*, an alternative explanation for the DLAV phenotype could be tricaine interfering with neuronal function, which in turn augments the effects of *svep1* knockdown. To test this possibility, we selectively blocked neuronal activity but not cardiac function by alpha-bungarotoxin mRNA injection [23], and quantified DLAV gap formation and lumenisation in comparison to, and in combination with, tricaine treatment [Figure 3C and D]. alpha-bungarotoxin had no effect on DLAV formation or lumenisation on its own, and did not augment the tricaine and *svep1* loss-of-function effects. These results suggest that the observed sensitization to *svep1* loss-of-function by tricaine is attributable to its effects on blood flow.

svep1 loss-of-function leads to a defect in tip/stalk cell specification in primary angiogenic sprouts.

The formation of the DLAV is initiated by the anastomosis of ipsilateral arterial sprouts, led by a tip cell [1]. To investigate tip cell identity in the zebrafish trunk, we took advantage of the recently published *Tg(apln:eGFP)* reporter line *[19]*, in which endothelial tip cells are highlighted by eGFP expression at 48 hpf. Following treatment with tricaine from 30 to 48 hpf, *svep1* morphants exhibited an expansion of *apln*+ endothelial cells in intersegmental vessels (ISVs), while control morphants predominantly presented *apln*+ cells in the dorsal-most region of the trunk vasculature, consistent with a contribution of tip cells to the formation of the DLAV (Figure 4A-D). In addition, *svep1* morphants presented an overall increase in *apln*+ cells per ISVs (56.5% ± 24 versus 17.8% ± 13.3 in control morphants) (Figure 4E).

As tip cell identity is in part characterised by increased levels of p-ERK downstream of Vegfa/Vegfr signalling, we next investigated this pathway activation in *svep1* morphants. Interestingly, sorted total endothelial cells from 48 hpf *svep1* morphants, treated with 1X tricaine from 30 hpf, did not show a significant increase in p-ERK levels normalised to total ERK levels (Figure 4F and G), suggesting that the increase of Vegfa/Vegfr signalling in the trunk ISV of *svep1* morphants is not ubiquitous across the endothelium. Overall, these results suggest that the DLAV phenotype present in *svep1* morphants treated with tricaine is associated with a defect in tip/stalk cell specification in primary angiogenic sprouts, potentially through the modulation of Vegfa/Vegfr signalling.

To verify that the observed defect in tip cell specification is not secondary to the further reduction in blood flow speed observed in *svep1* loss-of-function embryos we investigated tip cell identity in control embryos treated with 2X tricaine compared to 1X tricaine, as it results in a blood flow reduction greater than that observed in *svep1* loss-of-function embryos treated with 1X tricaine (451 μm/s ± 231.6, as presented by our laboratory in a recent manuscript [27], versus 521 μm/s ± 190). We found no differences between embryos treated with 1X and 2X tricaine (Figure 4H and I), suggesting that the defect in tip cell specification is primarily a consequence of *svep1* loss-of-function in reduced flow condition.

svep1 loss-of-function and knockdown are rescued by _flt1_ knockdown.

To investigate the functional relevance of this Vegfa/Vegfr signalling increase in *svep1* morphants, we decided to modulate it *in vivo*, first by targeting Flt1 expression. In mice and zebrafish, Flt1 mainly functions as a decoy receptor with high affinity for

Vegfa during development to modulate the activation of the Vegfa/Vegfr signalling pathway [21, 30, 31]**.** Alternative splicing of *flt1* generates two isoforms: a membrane bound form (mFlt1), and a soluble form (sflt1, an alternative spliced and secreted form of mFlt1) [32]. Reports have shown that sFlt1 acts as a negative regulator of tip cell formation in the zebrafish trunk [33].

To reduce *flt1* expression, we used a morpholino targeting both mFlt1 and sFlt1 expression. Similar to previous observations [21], *flt1* morphants do not exhibit any DLAV defects at 48 hpf when treated with tricaine from 30 to 48 hpf. However, in *svep1* mutants and morphants, knockdown of *flt1* expression led to a rescue of DLAV formation defects (Figure 5A, B). Interestingly, *flt1* knockdown rescued the DLAV segment lumenisation phenotype only in *svep1* morphants but not in mutant embryos (Figure 5C, D), suggesting potential differences in the expressivity of the *flt1* knockdown in *svep1* mutant and morphants.

In addition to the DLAV rescue, *flt1/svep1* double knockdown led to the formation of aberrant arterial loops in aISVs (18.5 % ± 12.4 versus 0.8% ± 2.7 in *MO-svep1* and 3.6% ± 6.1 in *MO-flt1* only) (Figure 5E, F). The majority of these arterial loops were lumenised and composed of more than one endothelial cell (>1 cell/loop: 94.1% in n=34 loops). In 9.3% of somites (26/280), we also observed abnormal aISVs to aISVs connections (Figure 5H), which were never seen in control embryos. Thus, the rescue of connectivity at the DLAV level through *flt1* knockdown produced an excess connectivity at aberrant locations.

Importantly, *flt1* morphants treated with 2X tricaine from 30-48 hpf exhibited aberrant arterial loops in only 2.4% ± 4.1 aISVs, while control morphants under the same treatment never exhibited any (N=3, n=21 *MO-flt1 1ng,* n=24 *MO-CTL 1ng*). In both conditions, we could not see any abnormal aISVs to aISVs connections. These results suggest that *svep1* loss-of-function, rather than reduced blood flow, is the principal driver for the excess connectivity observed with concomitant *flt1* knockdown.

In search for the underlying cause of hyperconnectivity, we next investigated tip cell specification. In embryos treated with 1X tricaine from 30 to 48hpf, *flt1* knockdown led to an expansion and increase of the total number of *apln*+ positive endothelial cells in aISVs, despite no significant DLAV formation defects (Figure 5I-K). *svep1/flt1* double morphants exhibit significantly more *apln*+ endothelial cells in the dorsal and ventral part of aISVs, and more *apln*+ cells per aISV than both *svep1* and *flt1* morphants alone (more than one *apln*+ cell in 87.6% ± 13.9 ISVs versus 70.3% ± 17.7 in *svep1* only morphants and 63.9 ± 21.9 in *flt1* only morphants)(Figure 5L).

These results suggest that the expansion of the number of tip cells in aISVs per se is not the driver of DLAV anastomosis defects, but potentially the cause for aberrant aISV to aISV connections.

Vegfa/Vegfr signalling is necessary for ISV lumenisation maintenance and DLAV formation

Vegfa/Vegfr signalling regulates primary angiogenic sprouting in the developing zebrafish trunk. Inhibition of Vegfr tyrosine kinase activation between 18 and 20 hpf results in the absence of angiogenic sprouting from the dorsal aorta [34]. However, to

our knowledge, there exist no reports for the role of active Vegfa/Vegfr signalling in the initial formation and lumenisation of the DLAV (30-48 hpf). As a polarised increase in Vegfa/Vegfr signalling is necessary to establish tip and stalk cells identity in the growing sprouts [6] and a local increase in VEGFA signalling is essential for the establishment of stable connections between vascular sprouts *in vivo* and *in vitro* [35], we decided to investigate the effect of a general reduction of this signalling pathway on the formation of a lumenised DLAV. For this purpose, we used the VEGFR2 inhibitor ZM323881, a tyrosine-kinase inhibitor that reduces Vegfa/Vegfr signalling [36], confirmed by down-regulation of p-ERK in FAC sorted endothelial cells from embryos treated with 50 nM ZM323881 and 1X tricaine from 30 to 48 hpf (Supplementary Figure 3A-B). Consistent with its function, ZM323881-mediated down regulation of Vegfa/Vegfr signalling can be partially rescued with down-regulation of *flt1* expression (Supplementary Figure 3E, F).

Embryos treated with 1X tricaine and 100 or 150 nM ZM323881 from 30 to 48 hpf exhibited significant DLAV defects (Supplementary Figure 3C, D).

Vegfa/Vegfr signalling inhibition exacerbates *svep1* loss-of-function DLAV phenotype in reduced flow conditions.

As the DLAV phenotype in *svep1* morphants correlates with an increase in Vegfa/Vegfr signalling and tip cell numbers (Figure 4), and because an expansion of tip cell numbers within aISVs does not result in ipsilateral anastomosis defect (Figure 5), we decided to investigate whether the increased Vegfa/Vegfr signalling observed in *svep1* morphants is correlative/compensatory or causative for the DLAV defects observed under reduced flow conditions.

We took advantage of the variability in expressivity of the DLAV phenotype observed in different reporter lines (Supplementary Figure 1) to select one presenting with a limited DLAV phenotype when injected with *svep1* morpholino and treated with 1X tricaine from 30 to 48 hpf. In this context, we find that concomitant treatment with 50 nM ZM323881 results in a significant increase in the number of gaps in the DLAV (20.3% ± 21.8 versus 5.4% ± 9.3) and in a reduction of the number of lumenised DLAV segments (35.4 ± 33.9 versus 76.9 ± 24.9) (Figure 6A-C). Similarly, we found that treatment with the commonly used VEGFR signalling inhibitor SU5416 [3, 12, 37, 38] also exacerbates the DLAV phenotype in *svep1* morphants treated with 1X tricaine from 30 to 48 hpf (supplementary Figure 5A-C).

Vegfr inhibition additionally impaired ISV lumenisation at 48 hpf (Figure 7A), suggesting that beyond its importance in the ipsilateral anastomosis of aISVs and DLAV lumenisation, Vegfa/Vegfr signalling is involved in the maintenance of aISV lumenisation status. Also *svep1* morphants exhibit a mild but significant reduction in ISV lumenisation that is increased by treatment with 50 nM ZM323881 (26.9% ± 22.6 versus 80.3% ± 16.5)) (Figure 7B). Furthermore, we find that concomitant *svep1* knockdown and Vegfa/Vegfr signalling inhibition leads to the emergence of embryos with a significant number of ISVs missing at 48 hpf (4.8% ± 9 versus 0.2 ± 1.3%), following treatment with ZM323881 and 1X tricaine from 30 to 48 hpf (Figure 7C). Finally, we find that in embryos treated with 50nM ZM323881 and 2X tricaine from 30 to 48 hpf, 40.9% ± 21 of ISVs are lumenised (compared to 26.9% ± 22.6 in mild *svep1 morphants* treated with 1X tricaine and 50nM Zm323881) and 3.3% ± 5.8 are missing at 48 hpf (compared to 26.9% ± 22.6 in mild *svep1 morphants* treated with 1X tricaine and 50nM Zm323881), suggesting that reduced *svep1* and reduced blood

flow both contribute to the emergence of a vascular phenotype in the context of Vegfa/Vegfr signalling inhibition (Figure 7D-G).

Overall, these results suggest that the increase in Vegfa/Vegfr signalling observed in *svep1* morphants under reduced flow conditions is not causative for the failure of ipsilateral aISVs to anastomose after 30 hpf, but potentially represents a compensatory effect. This is supported by the finding that Svep1 and Vegfa/Vegfr signalling appear to act synergistically to maintain vessel lumenisation and stability under low flow conditions.

Discussion

The question of how vessels anastomose remains incompletely understood, given the complexities of endogenous and exogenous signals driving vascular remodelling and development in parallel and sometimes synergistic ways [1]. Careful analysis of early-stage angiogenesis has shed light on the temporal and morphological dynamics underlying this process [11, 39, 40]. Following the establishment of a stable connection between neighbouring tip cells, supported by the local deposition of adherens junction proteins, such as VE-cadherin, F-actin and ZO-1 [40, 41], ISV connections become progressively lumenised. Lumenisation and stabilisation of ISV connections is thought to occur either through a flow-dependent transcellular hollowing of connecting tip cells (Type I anastomosis)[40, 42] or through a flow-independent process involving the coalescence of isolated luminal pockets into a single luminal space that will subsequently be perfused (Type II anastomosis)[39]. However, comparatively little is known about the molecular pathways leading to the formation and stabilisation of nascent anastomotic connections.

Here, we identified blood flow and Svep1 as regulators of vessel anastomosis in the developing zebrafish vasculature. Both appear to play a role in the stabilisation of nascent anastomotic connections between neighbouring vessels. Under reduced flow conditions, *svep1* knockdown or loss-of-function resulted in reduced anastomosis of ipsilateral ISVs and defective formation of a lumenised DLAV at 48 hpf. We find that endothelial cells in *svep1* morphants display increased Vegfa/Vegfr signalling, which is consistent with a concomitant increase in Apelin positive cells in ISVs. Neither of these events, however, appear causative, as the DLAV defect can be rescued with *flt1* knockdown and is exacerbated by Vegfa/Vegfr signalling inhibition. Interestingly, while inhibition of blood flow speed below that exhibited in a context of *svep1* loss-of-function and 1X tricaine treatment does similarly result in visible anastomosis defect in the DLAV region, these are not associated with a significant increase of Apelin positive cells in the trunk ISV. Therefore the expansion of the number of Apelin positive tip cells in aISVs is unlikely a consequence of the reduced anastomosis or lumenisation, and also per se not the causal driver of anastomosis defects. Our data rather suggest that the increased number of Apelin positive cells is related to the increased Vegfa/Vegfr signalling, as this is also seen in the *flt1* KD situation, and even exacerbated when both *svep1* and *flt1* are knocked down. Thus the increase in Vegfa/Vegfr signalling and Apelin positive tip cell numbers in the absence of *svep1* are likely compensatory, given that further increases of both in the flt1 KD condition can rescue the DLAV defects, whereas Vegfr inhibition exacerbates the loss of DLAV connections. In previous work in the mouse retina, Nesmith and colleagues have shown that endothelial cells presenting with reduced Flt1 expression were more likely to form stable connections with approaching sprouts [35]. They also clarified that reduced mFlt1 expression is what influences the bias towards stable connections, suggesting a cell-autonomous regulation of tip cell anastomosis. Finally, they

remarked that sprouts with reduced Flt1 expression exhibit reduced retraction of nascent connections with adjacent sprouts, proposing that this might lead to an increase in the number of suboptimal but stabilized new vascular connections. We noticed a significant increase of aberrant vascular loops within ISVs, which can functionally be considered suboptimal or redundant for perfusion of tissues, in embryos with reduced *svep1* and *flt1* expression compared to *flt1* knockdown alone. On its own, this result suggests that the role of Svep1 in vascular development might occur through the modulation of Flt1 activity in vivo. As the function of Flt1 in developmental angiogenesis appears strictly limited to its role as a decoy receptor for VEGFA [31, 43], we can speculate that Svep1 might support/enhance Flt1 decoy ability. However, under reduced flow conditions, while *flt1* knockdown enhances the formation of stable connections between ipsilateral neighbouring sprouts, we find that *svep1 knockdown* alone leads to a significant reduction in the stability of these connections. In addition, we find that inhibition of Vegfa/Vegfr signalling leads to a DLAV phenotype comparable to that observed in *svep1* mutant and morphants, in which Vegfa/Vegfr signalling levels are significantly upregulated, and that Vegfa/Vegfr inhibition in *svep1* morphants leads to a strong increase of anastomosis defects. Taken together, these results reinforce the conclusion that the observed increase in Vegfa/Vegfr signalling following *svep1* knockdown is compensatory in nature but insufficient to stabilise new connections in the absence of flow.

The importance of blood flow inhibition in the emergence of the DLAV phenotype might suggest a potential investigative avenue. In embryos with reduced blood flow and concomitant reduced Svep1 levels or reduced Vegfa/Vegfr signaling, we observed a significant reduction in ISV lumenisation. This suggest that in this context, a significant proportion of ISVs might initiate anastomosis through flow-independent

pathways (Type II anastomosis). We can speculate that blood flow plays a positive role in the stabilization of type II anastomosis between neighboring ISV, which would explain the DLAV formation defect observed in reduced (tricaine treatment) or abolished (*tnnt2a* morpholino) blood flow conditions. The significant increase in the DLAV phenotype observed in *svep1* loss-of-function and abolished flow conditions suggests a role of Svep1 in regulating vessel anastomosis in reduced flow conditions.

In addition, while blood flow reduction between 30 and 48 hpf is sufficient to induce anastomotic defects in the DLAV, this phenotype is significantly exacerbated with concomitant treatment with Vegfr signaling inhibitors, supporting the idea that both flow and Vegfa/Vegfr signaling may act synergistically to support stable vessel anastomosis.

Svep1 is a secreted ECM protein that has been reported to mediate cell to substrate adhesion in-vitro, in an integrin $\alpha 9\beta 1$-dependent manner [13]. Although integrin $\alpha 9$ zebrafish mutants fail to display a vascular phenotype other than a defect in lymphatic valve formation [44], interaction with another member of the Integrin family could prove more relevant. For example, Integrin $\beta 1$b appears to be important for the formation of the DLAV in zebrafish embryos [45]. Future efforts in identifying interaction partners for Svep1 will further enhance our understanding of the molecular pathways regulating vessel anastomosis. Imaging of the *svep1* reporter line *Tg(svep1: Gal4FF;UAS:GFP)* at 48 hpf showed strong GFP expression in dorsal epithelial cells, above the neural tube, and in individual neurons of the neural tube in close proximity to the anastomotic bridges forming between adjacent ISVs. We can speculate that neuronal expression of Svep1 is what locally regulates vessel

anastomosis, in a non-cell-autonomous manner. In addition, Svep1 is a multi-domain protein, the importance of each could be functionally tested in reduced flow conditions, by the generation of zebrafish lines expressing selective truncated forms of Svep1. Finally, the significant differences observed in *svep1* loss-of-function phenotype expressivity between zebrafish lines might offer an interesting avenue to decipher the compensatory mechanisms at play, and reveal new molecular pathways interacting with Svep1 in the regulation of vessel anastomosis. In the absence of clear structure-function details on Svep1 protein and knowledge of relevant molecular receptor interactions in endothelial cells, our mechanistic insights into how the non-endothelial expression of Svep1 supports vessel anastomosis remains very limited. Equally open remains the question whether there is a threshold of blood flow that is critical for stabilizing nascent anastomotic connections, and if so, whether this is similar in different vascular beds.

Understanding the genetic regulation of phenotypic robustness in angiogenesis and its failure [46] promises crucial insights into the mechanisms causing breakdown of vascular homeostasis in human disease. The search for genetic causes for vascular disease is particularly challenging due to multifactorial risk profiles and multigenic disease mechanisms. Interestingly however, Svep1 is evolutionarly highly conserved, and genotyping efforts by the Myocardial Infarction Genetics and CARDIoGRAM Exome Consortia identified missense variants in Svep1 associated with coronary artery disease and elevated blood pressure [47]. Svep1 loss-of-function mutations were also associated with worse outcome in septic shock [48]. Although the underlying mechanisms remain to be investigated, it is noteworthy that disturbed endothelial responses to flow are a central mechanism in artherosclerosis, and that vessel rarefaction due to breakdown of connectivity increases peripheral resistance,

and thus blood pressure. The link between Flt1 protein levels and reduced Vegfa/Vegfr signalling provides a well know mechanisms for vessel rarefaction and hypertension, for example in preeclampsia. Intriguingly, Svep1 mRNA is also strongly downregulated in cytotrophoblast populations in preeclampsia [49]. Future work will need to address whether our newly identified connection between blood flow and Svep1 function is involved in the pathomechanisms underlying vessel loss, coronary artery disease or other aspects of vascular dysfunction in humans.

Acknowledgments

We thank all members of the Gerhardt lab for interesting discussions and comments, as well as the Zebrafish facility staff at the MDC for excellent animal care.

Source of Funding

This work was supported by the DZHK (German Centre for Cardiovascular Research). B. Coxam was supported by a DZHK excellence Grant (Postdoc Start-up Grant – EX2-B DR_Coxam). This project and was supported by a grant from the Fondation Leducq (17 CVD 03) and from the DFG (CRC1348; Y.H. and S.S.-M. and CRC1366 as well as CRC1444; E.B.-K. and H.G).

Disclosure

None

References:

1. Hogan, B.M. and S. Schulte-Merker, *How to Plumb a Pisces: Understanding Vascular Development and Disease Using Zebrafish Embryos.* Dev Cell, 2017. **42**(6): p. 567-583.
2. Isogai, S., et al., *Angiogenic network formation in the developing vertebrate trunk.* Development, 2003. **130**(21): p. 5281-90.

3. Covassin, L.D., et al., *Distinct genetic interactions between multiple Vegf receptors are required for development of different blood vessel types in zebrafish.* Proc Natl Acad Sci U S A, 2006. **103**(17): p. 6554-9.
4. Covassin, L.D., et al., *A genetic screen for vascular mutants in zebrafish reveals dynamic roles for Vegf/Plcg1 signaling during artery development.* Dev Biol, 2009. **329**(2): p. 212-26.
5. Bussmann, J., et al., *Arteries provide essential guidance cues for lymphatic endothelial cells in the zebrafish trunk.* Development, 2010. **137**(16): p. 2653-7.
6. Shin, M., et al., *Vegfa signals through ERK to promote angiogenesis, but not artery differentiation.* Development, 2016. **143**(20): p. 3796-3805.
7. Bahary, N., et al., *Duplicate VegfA genes and orthologues of the KDR receptor tyrosine kinase family mediate vascular development in the zebrafish.* Blood, 2007. **110**(10): p. 3627-36.
8. Bussmann, J., et al., *Zebrafish VEGF receptors: a guideline to nomenclature.* PLoS Genet, 2008. **4**(5): p. e1000064.
9. Geudens, I. and H. Gerhardt, *Coordinating cell behaviour during blood vessel formation.* Development, 2011. **138**(21): p. 4569-83.
10. Siekmann, A.F. and N.D. Lawson, *Notch signalling limits angiogenic cell behaviour in developing zebrafish arteries.* Nature, 2007. **445**(7129): p. 781-4.
11. Betz, C., et al., *Cell behaviors and dynamics during angiogenesis.* Development, 2016. **143**(13): p. 2249-60.
12. Zygmunt, T., et al., *'In parallel' interconnectivity of the dorsal longitudinal anastomotic vessels requires both VEGF signaling and circulatory flow.* J Cell Sci, 2012. **125**(Pt 21): p. 5159-67.
13. Sato-Nishiuchi, R., et al., *Polydom/SVEP1 is a ligand for integrin alpha9beta1.* J Biol Chem, 2012. **287**(30): p. 25615-30.
14. Karpanen, T., et al., *An Evolutionarily Conserved Role for Polydom/Svep1 During Lymphatic Vessel Formation.* Circ Res, 2017. **120**(8): p. 1263-1275.
15. Morooka, N., et al., *Polydom Is an Extracellular Matrix Protein Involved in Lymphatic Vessel Remodeling.* Circ Res, 2017. **120**(8): p. 1276-1288.
16. Kimmel, C.B., et al., *Stages of embryonic development of the zebrafish.* Developmental dynamics : an official publication of the American Association of Anatomists, 1995. **203**(3): p. 253-310.
17. Lawson, N.D. and B.M. Weinstein, *In vivo imaging of embryonic vascular development using transgenic zebrafish.* Dev Biol, 2002. **248**(2): p. 307-18.
18. Traver, D., et al., *Transplantation and in vivo imaging of multilineage engraftment in zebrafish bloodless mutants.* Nature immunology, 2003. **4**(12): p. 1238-46.
19. Marin-Juez, R., et al., *Coronary Revascularization During Heart Regeneration Is Regulated by Epicardial and Endocardial Cues and Forms a Scaffold for Cardiomyocyte Repopulation.* Dev Cell, 2019. **51**(4): p. 503-515 e4.
20. Alestrom, P., et al., *Zebrafish: Housing and husbandry recommendations.* Lab Anim, 2019: p. 23677219869037.
21. Wild, R., et al., *Neuronal sFlt1 and Vegfaa determine venous sprouting and spinal cord vascularization.* Nat Commun, 2017. **8**: p. 13991.
22. Amigo, J.D., et al., *The role and regulation of friend of GATA-1 (FOG-1) during blood development in the zebrafish.* Blood, 2009. **114**(21): p. 4654-63.
23. Swinburne, I.A., et al., *Improved Long-Term Imaging of Embryos with Genetically Encoded alpha-Bungarotoxin.* PLoS One, 2015. **10**(8): p. e0134005.

24. Thisse, C. and B. Thisse, *High-resolution in situ hybridization to whole-mount zebrafish embryos.* Nat Protoc, 2008. **3**(1): p. 59-69.
25. Nuesslein-Volhard, C.D.R., *Zebrafish : a practical approach*. 2002, Oxford: Oxford University Press.
26. Schindelin, J., et al., *Fiji: an open-source platform for biological-image analysis.* Nat Methods, 2012. **9**(7): p. 676-82.
27. Geudens, I., et al., *Artery-vein specification in the zebrafish trunk is pre-patterned by heterogeneous Notch activity and balanced by flow-mediated fine-tuning.* Development, 2019. **146**(16).
28. Parmar, K.M., et al., *Integration of flow-dependent endothelial phenotypes by Kruppel-like factor 2.* J Clin Invest, 2006. **116**(1): p. 49-58.
29. Attili, S. and S.M. Hughes, *Anaesthetic tricaine acts preferentially on neural voltage-gated sodium channels and fails to block directly evoked muscle contraction.* PLoS One, 2014. **9**(8): p. e103751.
30. Ito, N., et al., *Identification of vascular endothelial growth factor receptor-1 tyrosine phosphorylation sites and binding of SH2 domain-containing molecules.* J Biol Chem, 1998. **273**(36): p. 23410-8.
31. Hiratsuka, S., et al., *Flt-1 lacking the tyrosine kinase domain is sufficient for normal development and angiogenesis in mice.* Proc Natl Acad Sci U S A, 1998. **95**(16): p. 9349-54.
32. Kendall, R.L. and K.A. Thomas, *Inhibition of vascular endothelial cell growth factor activity by an endogenously encoded soluble receptor.* Proc Natl Acad Sci U S A, 1993. **90**(22): p. 10705-9.
33. Krueger, J., et al., *Flt1 acts as a negative regulator of tip cell formation and branching morphogenesis in the zebrafish embryo.* Development, 2011. **138**(10): p. 2111-20.
34. Fish, J.E., et al., *Dynamic regulation of VEGF-inducible genes by an ERK/ERG/p300 transcriptional network.* Development, 2017. **144**(13): p. 2428-2444.
35. Nesmith, J.E., et al., *Blood vessel anastomosis is spatially regulated by Flt1 during angiogenesis.* Development, 2017. **144**(5): p. 889-896.
36. Whittles, C.E., et al., *ZM323881, a novel inhibitor of vascular endothelial growth factor-receptor-2 tyrosine kinase activity.* Microcirculation, 2002. **9**(6): p. 513-22.
37. Fong, T.A., et al., *SU5416 is a potent and selective inhibitor of the vascular endothelial growth factor receptor (Flk-1/KDR) that inhibits tyrosine kinase catalysis, tumor vascularization, and growth of multiple tumor types.* Cancer Res, 1999. **59**(1): p. 99-106.
38. De Angelis, J.E., et al., *Tmem2 Regulates Embryonic Vegf Signaling by Controlling Hyaluronic Acid Turnover.* Dev Cell, 2017. **40**(4): p. 421.
39. Herwig, L., et al., *Distinct cellular mechanisms of blood vessel fusion in the zebrafish embryo.* Curr Biol, 2011. **21**(22): p. 1942-8.
40. Lenard, A., et al., *In vivo analysis reveals a highly stereotypic morphogenetic pathway of vascular anastomosis.* Dev Cell, 2013. **25**(5): p. 492-506.
41. Phng, L.K., F. Stanchi, and H. Gerhardt, *Filopodia are dispensable for endothelial tip cell guidance.* Development, 2013. **140**(19): p. 4031-40.
42. Gebala, V., et al., *Blood flow drives lumen formation by inverse membrane blebbing during angiogenesis in vivo.* Nat Cell Biol, 2016. **18**(4): p. 443-50.
43. Fong, G.H., et al., *Role of the Flt-1 receptor tyrosine kinase in regulating the assembly of vascular endothelium.* Nature, 1995. **376**(6535): p. 66-70.

44. Shin, M., et al., *Valves Are a Conserved Feature of the Zebrafish Lymphatic System.* Dev Cell, 2019. **51**(3): p. 374-386 e5.
45. Iida, A., et al., *Integrin beta1 activity is required for cardiovascular formation in zebrafish.* Genes Cells, 2018. **23**(11): p. 938-951.
46. Kasper, D.M., et al., *MicroRNAs Establish Uniform Traits during the Architecture of Vertebrate Embryos.* Dev Cell, 2017. **40**(6): p. 552-565 e5.
47. Myocardial Infarction, G., et al., *Coding Variation in ANGPTL4, LPL, and SVEP1 and the Risk of Coronary Disease.* N Engl J Med, 2016. **374**(12): p. 1134-44.
48. Nakada, T.A., et al., *Identification of a nonsynonymous polymorphism in the SVEP1 gene associated with altered clinical outcomes in septic shock.* Crit Care Med, 2015. **43**(1): p. 101-8.
49. Gormley, M., et al., *Preeclampsia: novel insights from global RNA profiling of trophoblast subpopulations.* Am J Obstet Gynecol, 2017. **217**(2): p. 200 e1-200 e17.

Figures

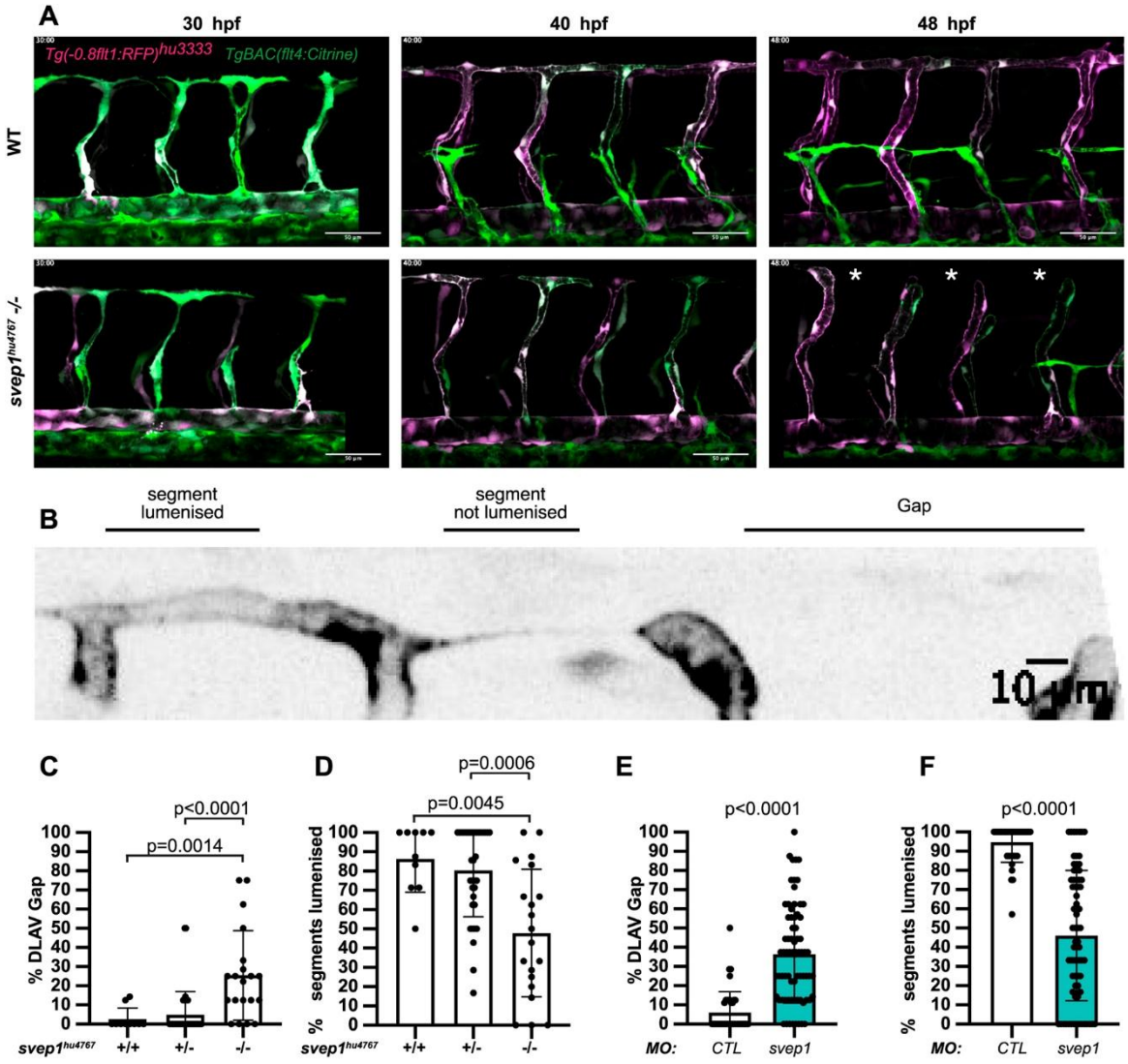

Figure 1 - *svep1* mutants and morphants zebrafish embryos exhibit vascular anastomosis defects.

(A) Stills from time lapse movie of *Tg(-0.8flt1:RFP)hu3333; TgBAC(flt4:Citrine)* embryos injected with *MO-CTL* (5ng) or *MO-svep1* (5ng) and treated with 1X (0.014%) tricaine from 30 to 48 hpf. White asterisks indicate gaps in the DLAV. **(B)** Still from a time lapse movie of a *Tg(-0.8flt1:RFP)^{hu3333}; TgBAC(flt4:Citrine)* embryo injected with *MO-CTL* (5ng) exhibiting a gap in the DLAV between two adjacent ISVs. Side view, dorsal side left. **(C)** Bilateral quantifications of the percentage of gaps in

the DLAV at 48 hpf in WT (n=5), *svep1*^{hu4767} heterozygous (n=18), and *svep1*^{hu4767} homozygous embryos (n=10) treated with 1X tricaine (0.014%) from 30 to 48 hpf (N=3). **(D)** Bilateral quantifications of the percentage of lumenised segments in the DLAV at 48 hpf in WT (n=5), *svep1*^{hu4767} heterozygous (n=18), and *svep1*^{hu4767} homozygous embryos (n=10) treated with 1X tricaine (0.014%) from 30 to 48 hpf (N=3). **(E)** Bilateral quantifications of the percentage of gaps in the DLAV at 48 hpf in embryos injected with *MO-CTL* (5 ng) (n=20) and *MO-svep1* (5ng) (n=36) and treated with 1X tricaine (0.014%) from 30 to 48 hpf (N=6). **(F)** Bilateral quantifications of the percentage of lumenised segments in the DLAV at 48 hpf in embryos injected with *MO-CTL* (5 ng) (n=20) and *MO-svep1* (5ng) (n=36) and treated with 1X tricaine (0.014%) from 30 to 48 hpf (N=6).

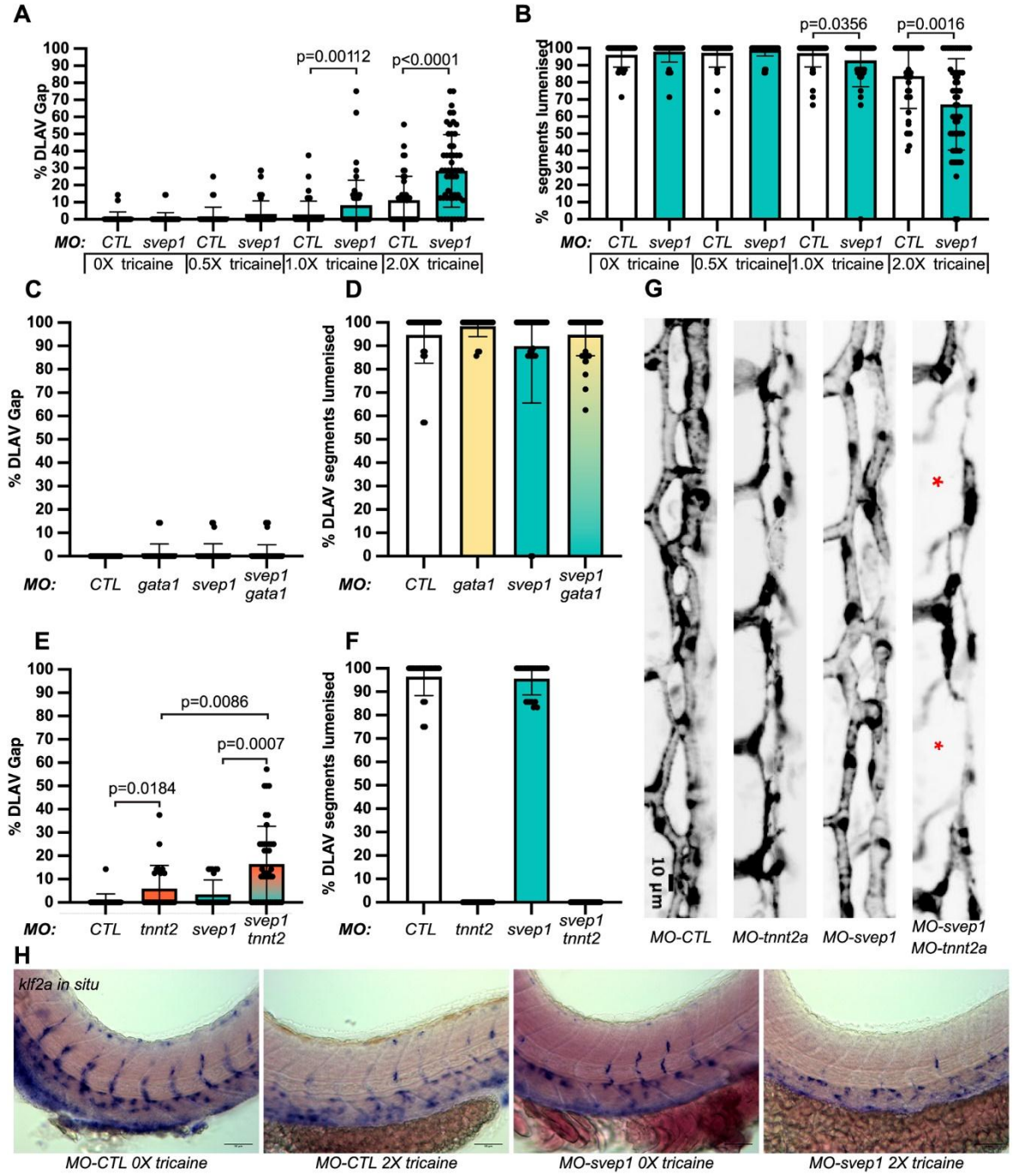

Figure 2 – *svep1* loss-of-function sensitises angiogenic remodelling to reduced blood flow.

(A) Bilateral quantifications of the percentage of gaps in the DLAV at 48 hpf in embryos injected with *MO-CTL* (5 ng) and *MO-svep1* (5ng) and treated with 0X (n=14 *MO-CTL*, n=20 *MO-svep1*), 0.5X (n=16 *MO-CTL*, n=24 *MO-svep1*), 1X (n=22 *MO-CTL*, n=27 *MO-svep1*) or 2X (n=21 *MO-CTL*, n=27 *MO-svep1*) from 30 to 48 hpf (N=3). **(B)** Bilateral quantifications of the percentage of lumenised segments in the

DLAV at 48 hpf in embryos injected with *MO-CTL* (5 ng) and *MO-svep1* (5ng) and treated with 0X (n=14 *MO-CTL*, n=20 *MO-svep1*), 0.5X (n=16 *MO-CTL*, n=24 *MO-svep1*), 1X (n=22 *MO-CTL*, n=27 *MO-svep1*) or 2X (n=21 *MO-CTL*, n=27 *MO-svep1*) from 30 to 48 hpf (N=3). **(C)** Bilateral quantifications of the percentage of gaps in the DLAV at 48 hpf in embryos injected with *MO-CTL* (5 ng) (n=13), *MO-gata1* (8ng) (n=12), *MO-svep1* (5ng) (n=16) and *MO-gata1* (8ng)/*MO-svep1* (5ng) (n=25) (N=3). **(D)** Bilateral quantifications of the percentage of lumenised segments in the DLAV at 48 hpf in embryos injected with *MO-CTL* (5 ng) (n=13), *MO-gata1* (8ng) (n=12), *MO-svep1* (5ng) (n=16) and *MO-gata1* (8ng)/*MO-svep1* (5ng) (n=25) (N=3). **(E)** Bilateral quantifications of the percentage of gaps in the DLAV at 48 hpf in embryos injected with *MO-CTL* (5 ng) (n=11), *MO-tnnt2a* (4ng) (n=12), *MO-svep1* (5ng) (n=12) and *MO-tnnt2a* (4ng)/MO-svep1 (5ng) (n=21) (N=3). **(F)** Bilateral quantifications of the percentage of lumenised segments in the DLAV at 48 hpf in embryos injected with *MO-CTL* (5 ng) (n=11), *MO-tnnt2a* (8ng) (n=12), *MO-svep1* (5ng) (n=12) and *MO-tnnt2a* (4ng)/*MO-svep1* (5ng) (n=21) (N=3). **(G)** Maximum intensity projection of dorsal view of the DLAV from representative embryos injected with *MO-CTL* (5 ng) (n=11), *MO-tnnt2a* (8ng) (n=12), *MO-svep1* (5ng) (n=12) and *MO-tnnt2a* (4ng)/MO-svep1 (5ng) (n=21) embryos at 48 hpf. Red asterisks indicate gaps. **(H)** Bright field images of *klf2a in situ* hybridization of 48 hpf embyos injected with *MO-CTL* or *MO-svep1* and treated with 0X or 2X tricaine from 30-48hpf.

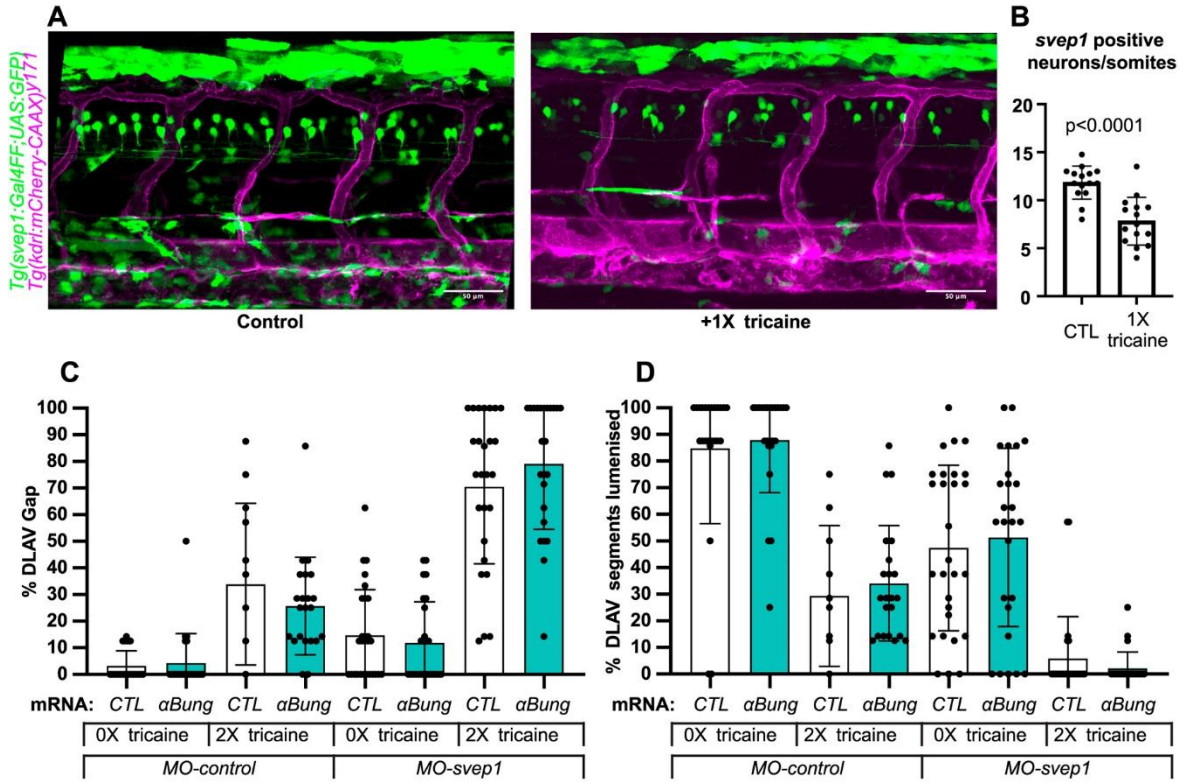

Figure 3 - *svep1* is expressed in neurons in the neural tube.

(A) Representative images of 48 hpf *Tg(svep1:Gal4FF; UAS:eGFP); Tg(kdrl:mcherry-CAAX)*^{y171} embryos with or without treatment with 1X (0.014%) tricaine from 30 to 48 hpf. **(B)** Quantification of average numbers of *Tg(svep1:Gal4FF; UAS:eGFP)* positive neurons in the neural tube area of 48 hpf embryos with or without treatment with 1X (0.014%0 tricaine from 30 to 48 hpf. (N=3, n=15 controls, n=16 treated **(C)** Bilateral quantifications of the percentage of gaps in the DLAV at 48 hpf in embryos injected with control mRNA (GFP, 50pg) or α-bungarotoxin mRNA, *MO-CTL* (5 ng) or *MO-svep1* (5ng), and treated with 0X or 2X tricaine from 30-48hpf. (N=2, n=24-28) **(D)** Bilateral quantifications of the percentage of lumenised segments in the DLAV at 48 hpf in embryos injected with control mRNA (GFP, 50pg) or α-bungarotoxin mRNA, *MO-CTL* (5 ng) or *MO-svep1* (5ng) and treated with 0X or 2X tricaine from 30-48hpf (N=2, n=24-28).

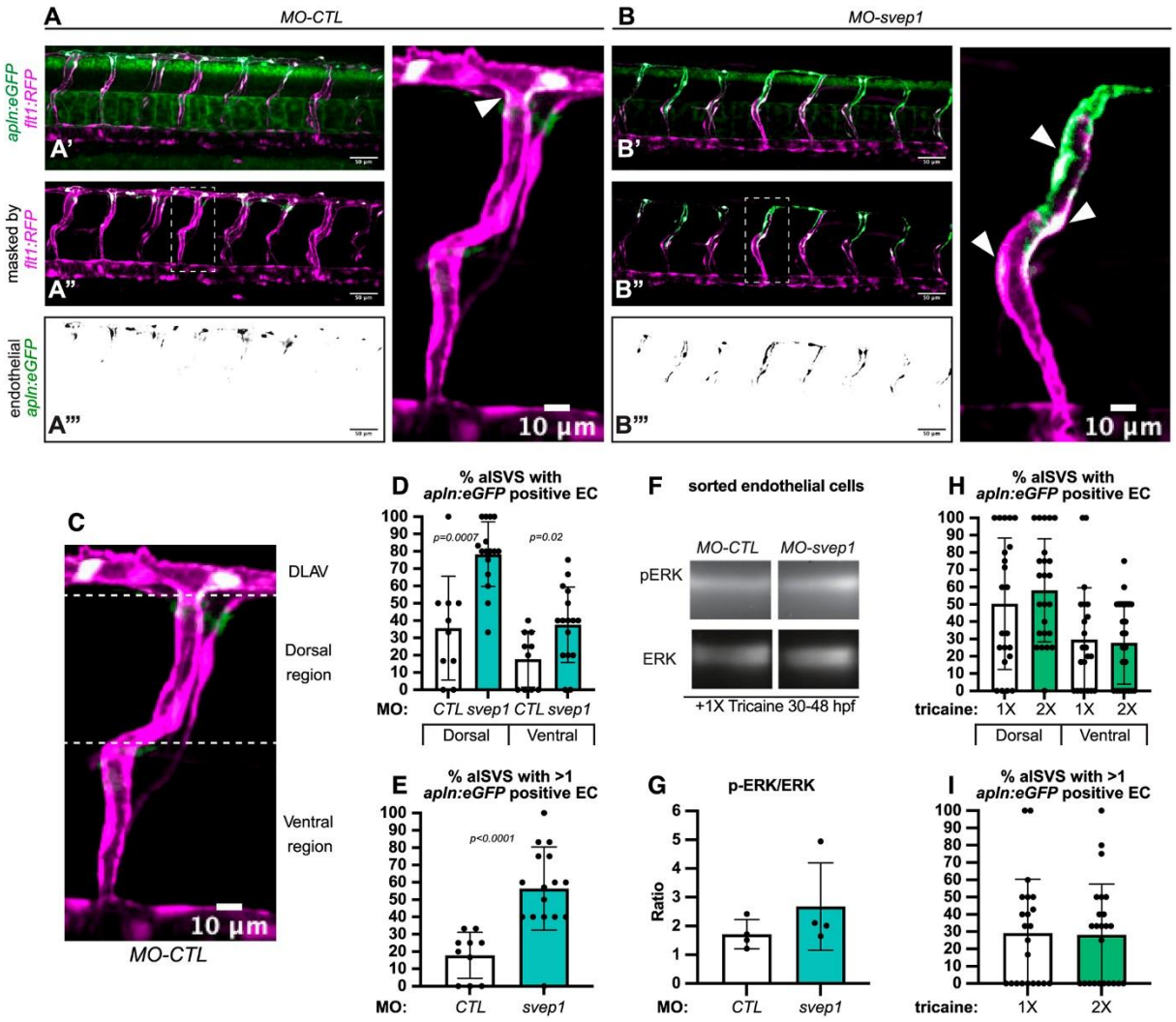

Figure 4 - *svep1* loss-of-function leads to a defect in tip/stalk cell specification in primary angiogenic sprouts.

(A) Maximum intensity projection of a representative *TgBAC(apln:eGFP)bns157, Tg(-0.8flt1:RFP)hu5333 MO-CTL* (5ng) embryo. C' shows the unprocessed maximum intensity projection, C'' shows the GFP signal volume-masked by the RFP signal, to limit detection to the endothelium, and C''' shows the resulting endothelial GFP signal only. **(B)** Maximum intensity projection of a representative *TgBAC(apln:eGFP)bns157, Tg(-0.8flt1:RFP)hu5333 MO-CTL* (5ng) embryo. D' shows the unprocessed maximum intensity projection, D'' shows the GFP signal

volume-masked by the RFP signal, to limit detection to the endothelium, and D''' shows the resulting endothelial GFP signal only. **(C)** Maximum intensity projection of a MO-CTL (5ng) aISV at 48 hpf, highlighting the ventral and dorsal region used for further quantifications in **D** and **E**. **(D)** Quantification of the percentage of aISVs with *apln:eGFP* positive endothelial cells in the (1) dorsal and (2) ventral region in 48 hpf MO-CTL (5ng) (n=10) and *MO-svep1*(5ng) (n=16) morphant embryos treated with 1X (0.014%) tricaine from 30 to 48 hpf (N=3). **(E)** Quantification of the percentage of aISVs with more than one *apln:eGFP* positive endothelial cells in 48 hpf *MO-CTL* (5ng) (n =10) and *MO-svep1* (5ng) (n=16) morphant embryos treated with 1X (0.014%) tricaine from 30 to 48 hpf (N=3). **(F)** Representative image of p-ERK and ERK levels in FAC sorted endothelial cells from *MO-CTL* (5ng) and *MO-svep1* (5ng) morphants at 48hpf, treated with 1X (0.014%) tricaine from 30 to 48 hpf (N=4). **(G)** Quantification of p-ERK in FAC sorted endothelial cells of *MO-CTL* (5ng) and *MO-svep1* (5ng) morphants at 48hpf, treated with 1X (0.014%) tricaine from 30 to 48 hpf. Expression levels were normalised to total ERK levels (N=4). **(H)** Quantification of the percentage of aISVs with *apln:eGFP* positive endothelial cells in the (1) dorsal and (2) ventral region in 48 hpf embryos treated with 1X (0.014%)(n=22) or 2X (0.028%)(n=24) tricaine from 30 to 48 hpf (N=3). **(I)** Quantification of the percentage of aISVs with more than one *apln:eGFP* positive endothelial cells in 48 hpf embryos treated with 1X (0.014%)(n=22) or 2X (0.028%)(n=24) tricaine from 30 to 48 hpf (N=3).

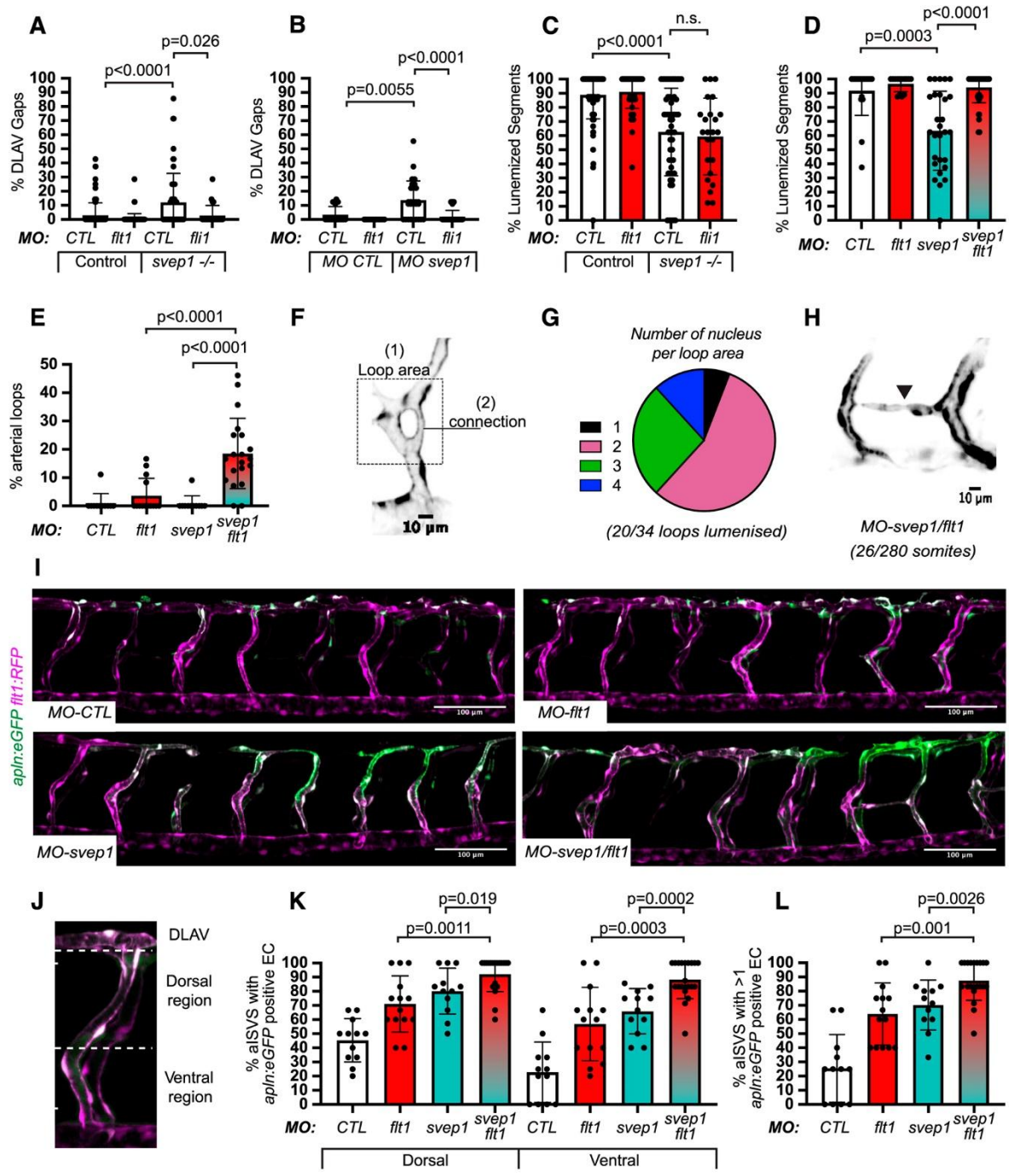

Figure 5 – *svep1* loss-of-function and knockdown are rescued by *flt1* knockdown.

(A) Bilateral quantifications of the percentage of gaps in the DLAV at 48 hpf in controls and *svep1*^{hu4767} -/- embryos injected with *MO-CTL* (5ng) (n= 45 and n=27 respectively) or *MO-flt1* (1ng) (n=50 and n=12 respectively), and treated with 1X

tricaine from 30 to 48 hpf (N=3). **(B)** Bilateral quantifications of the percentage of gaps in the DLAV at 48 hpf in *MO-CTL* (5 ng) (n=9), *MO-flt1* (1ng) (n=7), *MO-svep1* (5ng) (n=14) and *MO-flt1* (1ng)/*MO-svep1* (5ng) (n=25) embryos (N=3), and treated with 1x tricaine from 30-48 hpf. **(C)** Bilateral quantifications of the percentage of lumenised segments in the DLAV at 48 hpf in controls and mutant *svep1*$^{512-/-}$ injected with *MO-CTL* (5ng) (n= 45 and n=27 respectively) or *MO-flt1* (1ng) (n=50 and n=12 respectively), and treated with 1X tricaine from 30 to 48 hpf (N=3). **(D)** Bilateral quantifications of the percentage of lumenised segments in the DLAV at 48 hpf in *MO-CTL* (5 ng) (n=9), *MO-flt1* (1ng) (n=7), *MO-svep1* (5ng) (n=14) and *MO-flt1* (1ng)/MO-svep1 (5ng) (n=25) embryos (N=3). **(E)** Bilateral quantifications of the percentage of aISV loops at 48 hpf in *MO-CTL* (5 ng) (n=11), *MO-flt1* (1ng) (n=14), *MO-svep1* (5ng) (n=11) and *MO-flt1* (1ng)/*MO-svep1* (5ng) (n=20) embryos (N=3). **(F)** Representative image of an arterial aISV loop in *MO-svep1*(5ng)/*MO-flt1*(1ng) *Tg(-0.8flt1:RFP)*^{hu3333} embryos at 48 hpf, treated with 1X(0.014%) tricaine from 30 to 48 hpf. **(G)** Quantification of number of nucleus per loop area (see figure 4F) at 48 hpf in *MO-svep1*(5ng)/*MO-flt1*(1ng) embryos at 48 hpf, treated with 1X (0.014%) tricaine from 30 to 48 hpf (n=34 loops counted. 2, 19, 9 and 4 loops had 1, 2, 3 or 4 nucleus per loop area, respectively). 20/34 loops were lumenised) (N=3) **(H)** Representative image of an aISV to aISV connection in the region of the horizontal myoseptum at 48 hpf in in *MO-svep1*(5ng)/*MO-flt1*(1ng) *Tg(-0.8flt1:RFP)*^{hu3333} embryos at 48 hpf, treated with 1X (0.014%) tricaine from 30 to 48 hpf. (n=20 fish, 26 connections visible out of 280 somites, 8/26 connections were lumenised, N=3). **(I)** Maximum intensity projection of a representative *TgBAC(apln:eGFP)*^{bns157}, *Tg(-0.8flt1:RFP)*^{hu5333} morphant embryos at 48 hpf. The panels show the GFP signal volume-masked by the RFP signal, to limit detection to the endothelium in *MO-CTL* (5ng), *MO-flt1* (1ng), *MO-svep1* (5ng) and *MO-svep1* (5ng) /*MO-flt1* (1ng) embryos

treated with 1X (0.014%) tricaine from 30 to 48 hpf. **(J)** Maximum intensity projection of a *MO-svep1* (5ng)/*MO-flt1* (1ng) aISV at 48 hpf, highlighting the ventral and dorsal region used for further quantifications in (K). **(K)** Quantification of the percentage of aISVs with *apln:eGFP* positive endothelial cells in the (1) dorsal and (2) ventral region in 48 hpf *MO-CTL* (5ng) (n=12), *MO-flt1* (1ng) (n=14), *MO-svep1* (5ng)(n=12) and *MO-svep1*(5ng)/*MO-flt1* (1ng) (n=20) morphant embryos treated with 1X (0.014%) tricaine from 30 to 48 hpf (N=3). **(L)** Quantification of the percentage of aISVs with more than one *apln:eGFP* positive endothelial cells in 48 hpf *MO-CTL* (5ng) (n=12),*MO-flt1* (1ng) (n=14), *MO-svep1* (5ng)(n=12) and *MO-svep1* (5ng)/*MO-flt1* (1ng) (n=20) morphant embryos treated with 1X (0.014%) tricaine from 30 to 48 hpf (N=3).

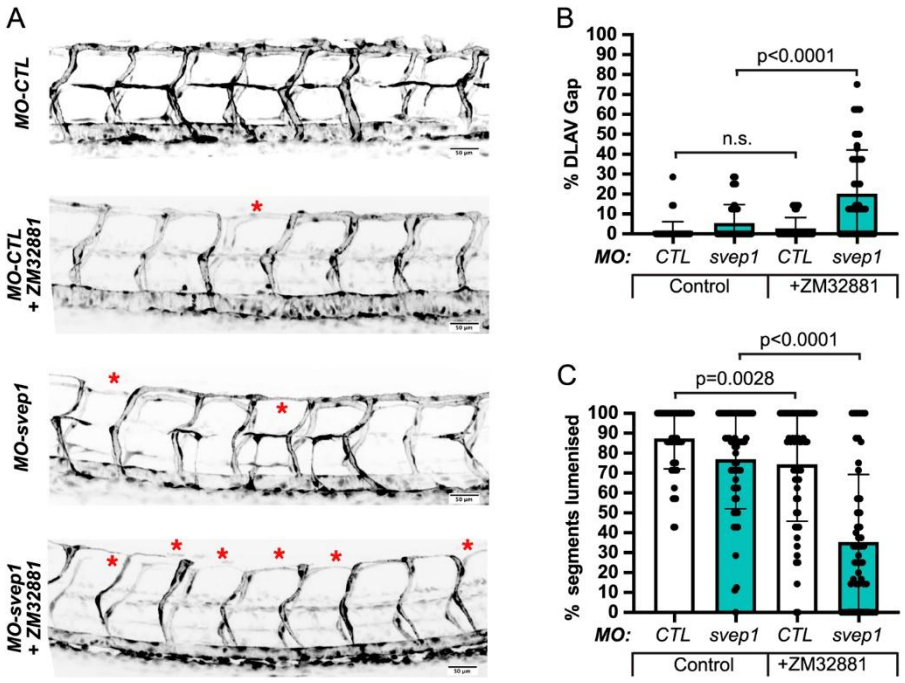

Figure 6 – Vegfa/Vegfr signalling is necessary for ISV lumenisation maintenance and DLAV formation

(A) Maximum intensity projections at 48 hpf of the trunk of MO-CTL (5ng) and MO-svep1 (5ng), Tg(fli1a:eGFP)y7 embryos, treated with 1X (0.014%) tricaine, with or without 50ng ZM32881. (B) Bilateral quantifications of the percentage of gaps in the DLAV at 48 hpf in MO-CTL (5 ng) (n=29 (0nM ZM32881), n=28 (50nM ZM32881)) MO-svep1 (5ng) (n=29 (0 nM ZM32881), n=26 (50nM ZM32881)) embryos treated with 1X (0.014%) tricaine and 0 or 50 nM ZM32881 from 30 to 48 hpf, (N=3). **(C)** Bilateral quantifications of the percentage of lumenised segments in the DLAV at 48 hpf in *MO-CTL* (5 ng) (n=29 (0nM ZM32881), n=28 (50nM ZM32881)) *MO-svep1* (5ng) (n=29 (0 nM ZM32881), n=26 (50nM ZM32881)) embryos treated with 1X (0.014%) tricaine and 0 or 50 nM ZM32881 from 30 to 48 hpf (N=3).

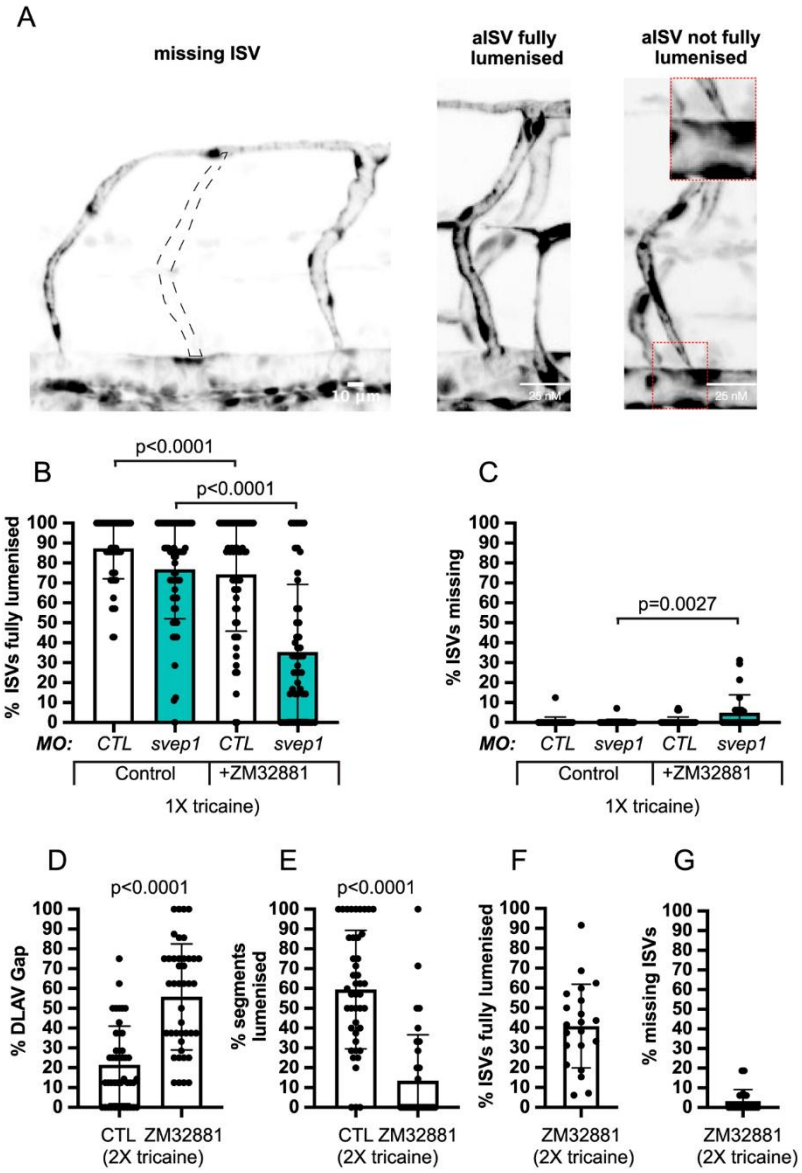

Figure 7 – Vegfa/Vegfr signalling is necessary for ISV lumenisation maintenance and DLAV formation

(A) Representative images of missing ISVs, fully lumenised ISV and not fully lumenised ISV at 48 hpf. Quantifications of these phenotypes are presented in (B and C). **(B)** Bilateral quantifications of the percentage of missing ISVs in the trunk of 48 hpf *MO-CTL* (5 ng) (n=29 (0nM ZM32881), n=28 (50nM ZM32881)) *MO-svep1* (5ng) (n=29 (0 nM ZM32881), n=26 (50nM ZM32881)) embryos treated with 1X (0.014%) tricaine and 0 or 50 nM ZM32881 from 30 to 48 hpf (N=3). **(D)** Bilateral

quantifications of the percentage of ISVs lumenised dorsally to ventrally in the trunk of 48 hpf *MO-CTL* (5 ng) n=29 (0nM ZM32881), n=28 (50nM ZM32881)) *MO-svep1* (5ng) n=29 (0 nM ZM32881), n=26 (50nM ZM32881)) embryos treated with 1X (0.014%) tricaine and 0 or 50 nM ZM32881 from 30 to 48 hpf (N=3). **(D)** Bilateral quantifications of the percentage of gaps in the DLAV at 48 hpf in embryos treated with 2X (0.028%) tricaine and 0 (n=22)or 50 nM (n=21) ZM32881 from 30 to 48 hpf, (N=3). **(E)** Bilateral quantifications of the percentage of lumenised segments in the DLAV at 48 hpf in embryos treated with 2X (0.028%) tricaine and 0 (n=22)or 50 nM (n=21) ZM32881 from 30 to 48 hpf, (N=3) **(F)** Bilateral quantifications of the percentage of missing ISVs in the trunk of 48 hpf in embryos treated with 2X (0.028%) tricaine and 50 nM (n=21) ZM32881 from 30 to 48 hpf, (N=3). **(G)** Bilateral quantifications of the percentage of ISVs lumenised dorsally to ventrally in the trunk of 48 hpf in embryos treated with 2X (0.028%) tricaine and 50 nM (n=21) ZM32881 from 30 to 48 hpf, (N=3).

Supplementary Figure 1

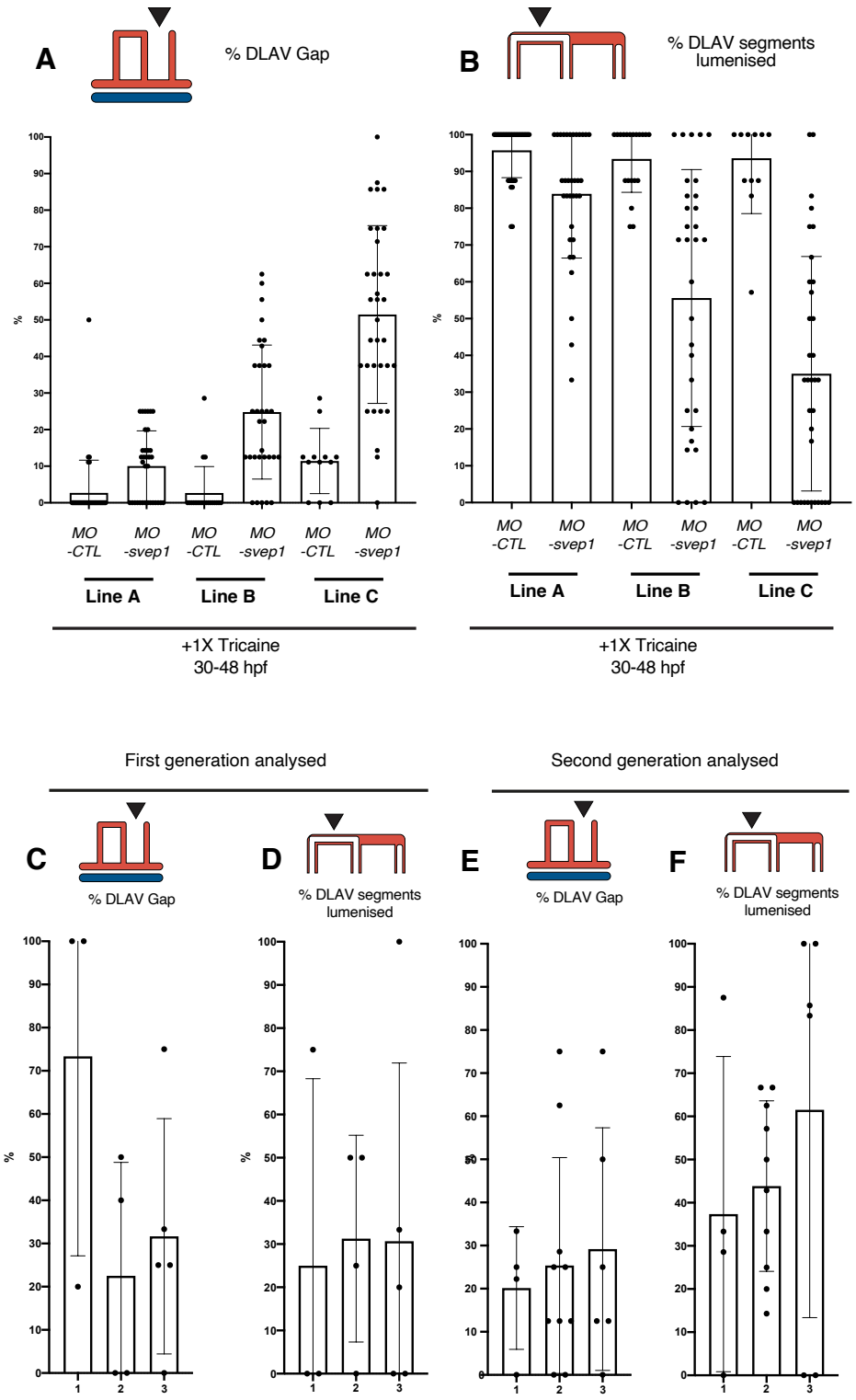

Fig. S1. (A) Bilateral quantifications of the percentage of gaps in the DLAV at 48 hpf in Line A: *Tg(fli1a:eGFP)y1* (N=3, n=18 *MO-CTL* 5ng, n=17 *MO-svep1* 5ng), Line B: *TgBAC(apln:eGFP); Tg(-0.8flt1:RFP)* (N=3, n=10 *MO-CTL* 5ng, n=16 *MO-svep1* 5ng), Line C: *TgBAC(flt1:YFP), Tg(kdrl:mCherry)* (N=3, n=6 *MO-CTL* 5ng, n=17 *MO-svep1* 5ng). The embryos were treated with 1X (0.014%) tricaine from 30 to 48 hpf.

(B) Bilateral quantifications of the percentage of lumenised segments in the DLAV at 48 hpf in Line A: *Tg(fli1a:eGFP)y1* (N=3, n=18 *MO-CTL* 5ng, n=17 *MO-svep1* 5ng), Line B: *TgBAC(apln:eGFP); Tg(-0.8flt1:RFP)* (N=3, n=10 *MO-CTL* 5ng, n=16 *MO-svep1* 5ng), Line C: *TgBAC(flt1:YFP), Tg(kdrl:mCherry)* (N=3, n=6 *MO-CTL* 5ng, n=17 *MO-svep1* 5ng). The embryos were treated with 1X (0.014%) tricaine from 30 to 48 hpf.

(C) Unilateral quantifications of the percentage of gaps in the DLAV at 48 hpf in *svep1*^{hu4767} homozygous mutants (n=3, 4, 5 embryos) treated with 1X tricaine (0.014%) from 30 to 48 hpf.

(D) Unilateral quantifications of the percentage of lumenised segments in the DLAV at 48 hpf in *svep1*^{hu4767} homozygous mutants (n=3, 4, 5 embryos) treated with 1X tricaine (0.014%) from 30 to 48 hpf.

(E) Bilateral quantifications of the percentage of gaps in the DLAV at 48 hpf in *svep1*^{hu4767} (n=2, 5, 3 embryos) treated with 1X tricaine (0.014%) from 30 to 48 hpf (N=3).

(F) Bilateral quantifications of the percentage of lumenised segments in the DLAV at 48 hpf in *svep1*^{hu4767} homozygous mutants (n=2, 5, 3 embryos) treated with 1X tricaine (0.014%) from 30 to 48 hpf (N=3).

Supplementary Figure 2

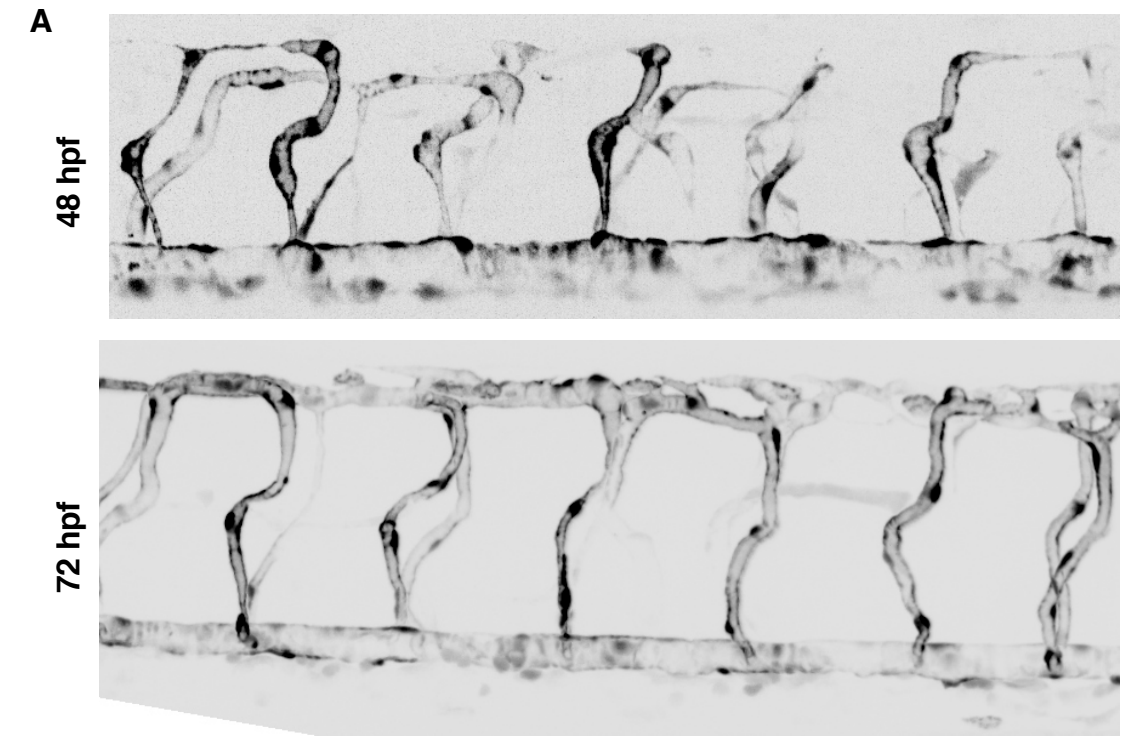

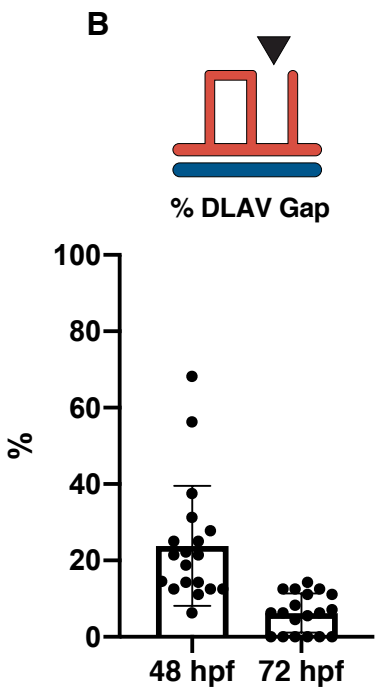

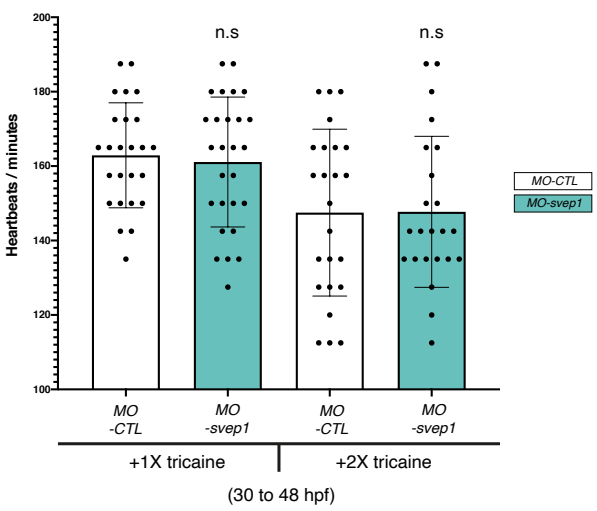

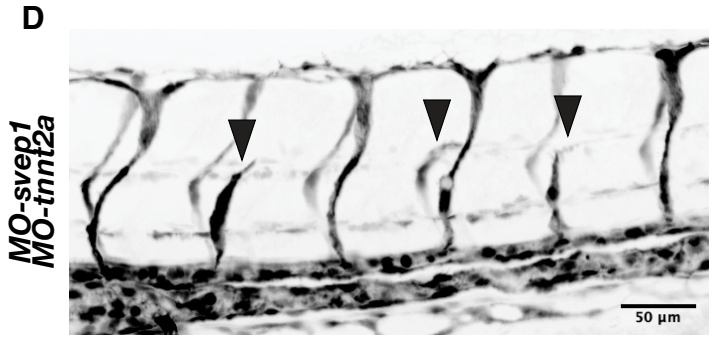

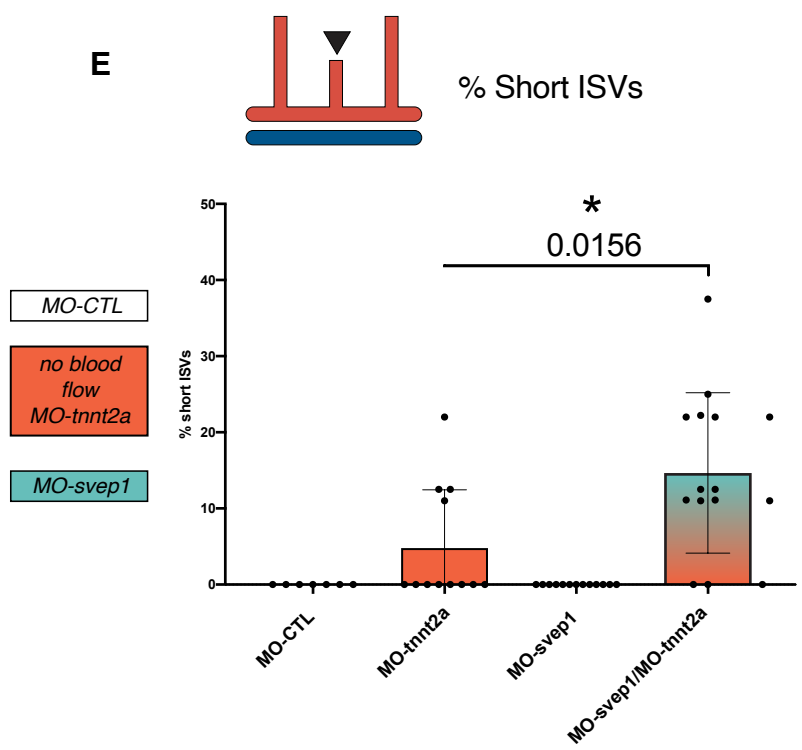

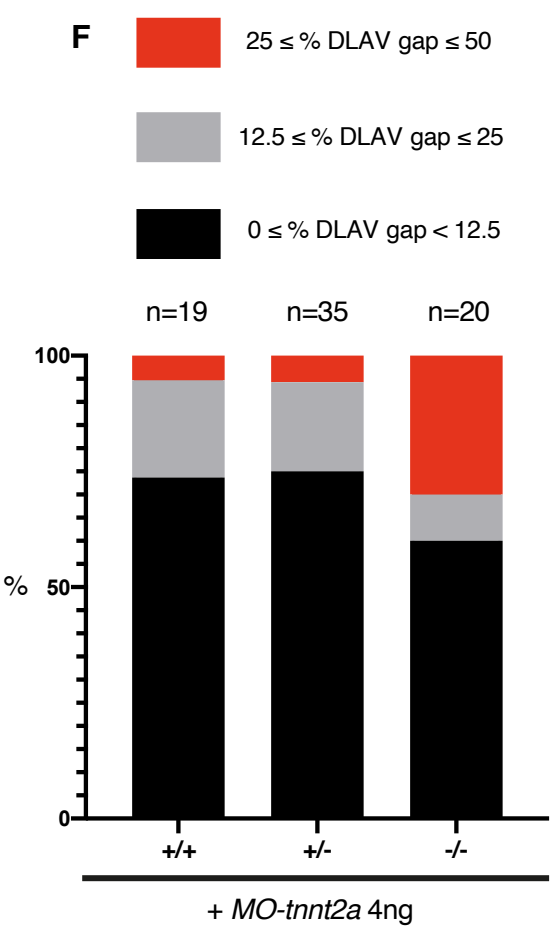

Fig. S2. (A) Representative image of a *Tg(-0.8flt1:RFP)*^{hu333}, svep1$^{hu4767\ -/-}$ embryo treated with 1X (0.014%) tricaine from 30 to 48 hpf and imaged at 48 and 72 hpf.

(B) Bilateral quantification of the percentage of gaps at 48 and 72 hpf in the DLAV of svep1$^{hu4767\ -/-}$ embryo treated with 1X (0.014%) tricaine from 30 to 48 hpf (n=19, N=3).

(C) Quantification of heart rate (heartbeats/minute) in the dorsal aorta of *Tg[gata1a:dsRed]*^{sd} MO-CTL (5ng) or MO-svep1 (5ng) embryos at 48 hpf, treated with 1X (0.014%)or 2X (0.028%) tricaine from 30 hpf. (N=4, n=25, 24 MO-CTL (1x, 2X), n=27, 23 MO-svep1 (1X, 2X)).

(D) Maximum intensity projection of zebrafish trunk in MO-svep1 (5ng)/Mo-tnnt2a (4ng) embryo at 48 hpf. black arrowheads indicate short ISVs.

(E) Bilateral quantification of the percentage of short ISVs in the trunk of 48 hpf MO-CTL (5ng)(n=7), MO-tnnt2a (4ng)(n=12), MO-svep1 (5ng)(n=13) and MO-svep1(5ng)/MO-tnnt2a (4ng)(n=15) embryos (N=3).

(F) Percentage of fish presenting with less than 12.5%, between 12.5 and 25% or above 25% gaps in the DLAV at 48 hpf in *svep1*$^{+/+}$ (n=19) , *svep1*$^{+/-}$ (n=35) or *svep* $^{-/-}$ (n=20) embryos injected with *MO-tnnt2a* (4ng) (N=4).

Supplementary Figure 3

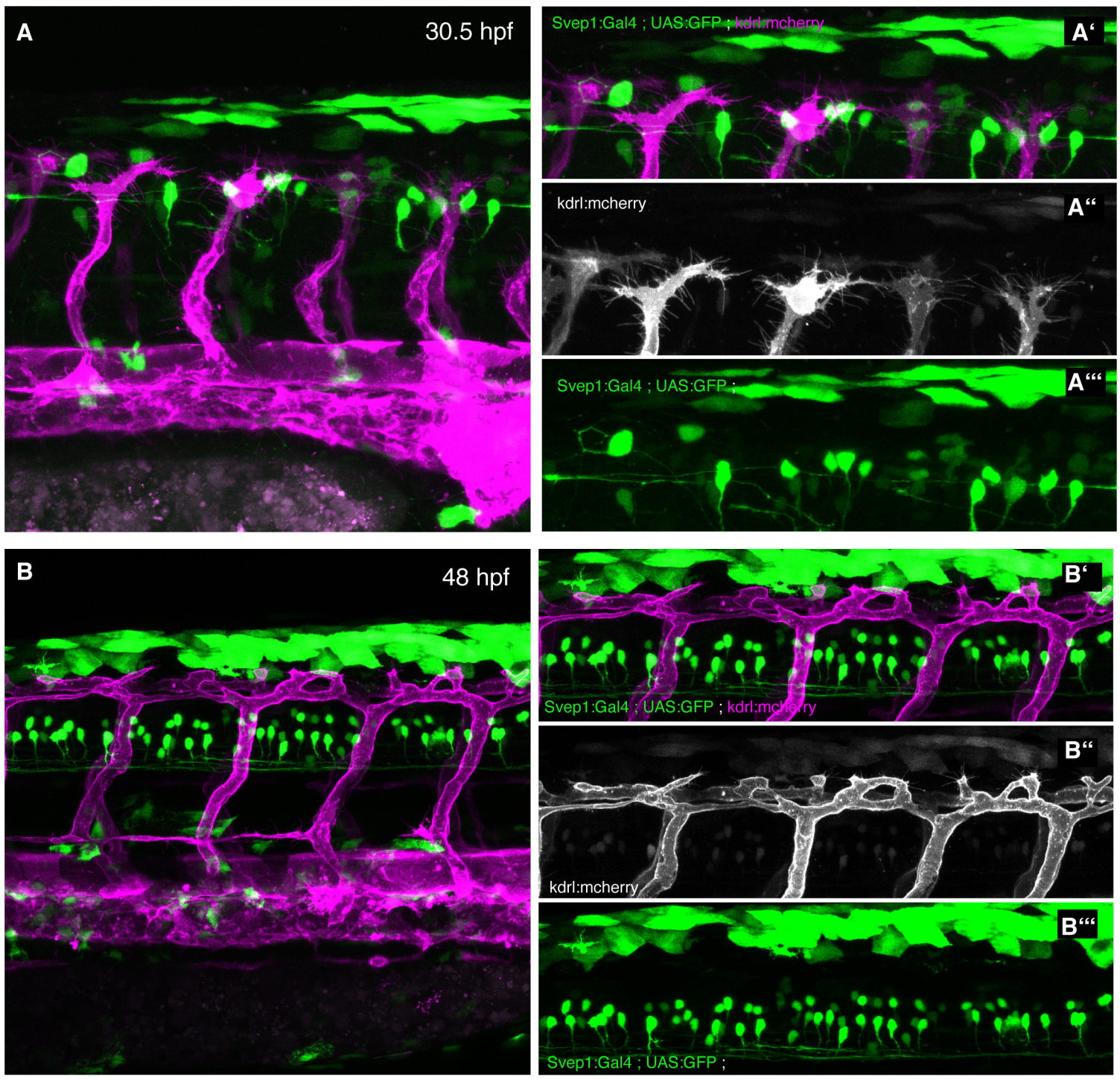

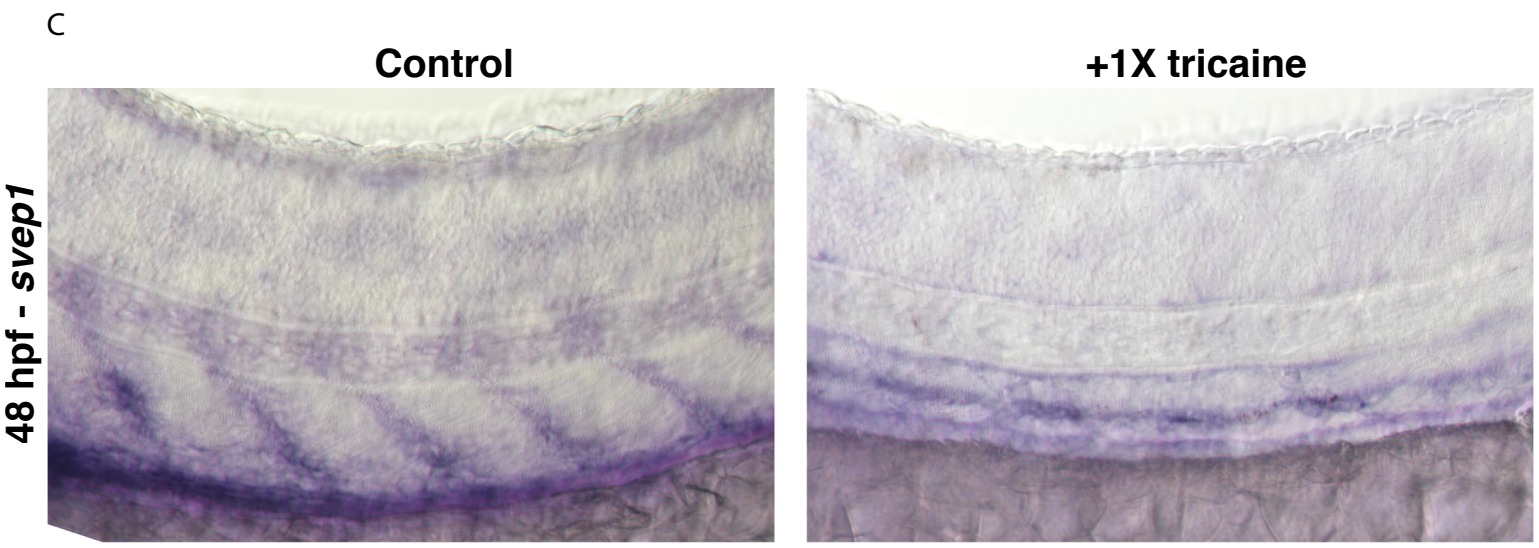

Fig. S3. (A) Representative images of 48 hpf *Tg(svep1:Gal4FF; UAS:eGFP); Tg(kdrl:mcherry-CAAX)^{y171}* in the trunk of embryos at 30.5 hpf.

(B) Representative images of 48 hpf *Tg(svep1:Gal4FF; UAS:eGFP); Tg(kdrl:mcherry-CAAX)^{y171}* in the trunk of embryos at 48 hpf.

(C) *In-situ svep1* endogenous expression in 48hpf embryos not treated (n=11) or treated with 1X (0.0168%) tricaine from 30 to 48 hpf (n=18).

Supplementary Figure 4

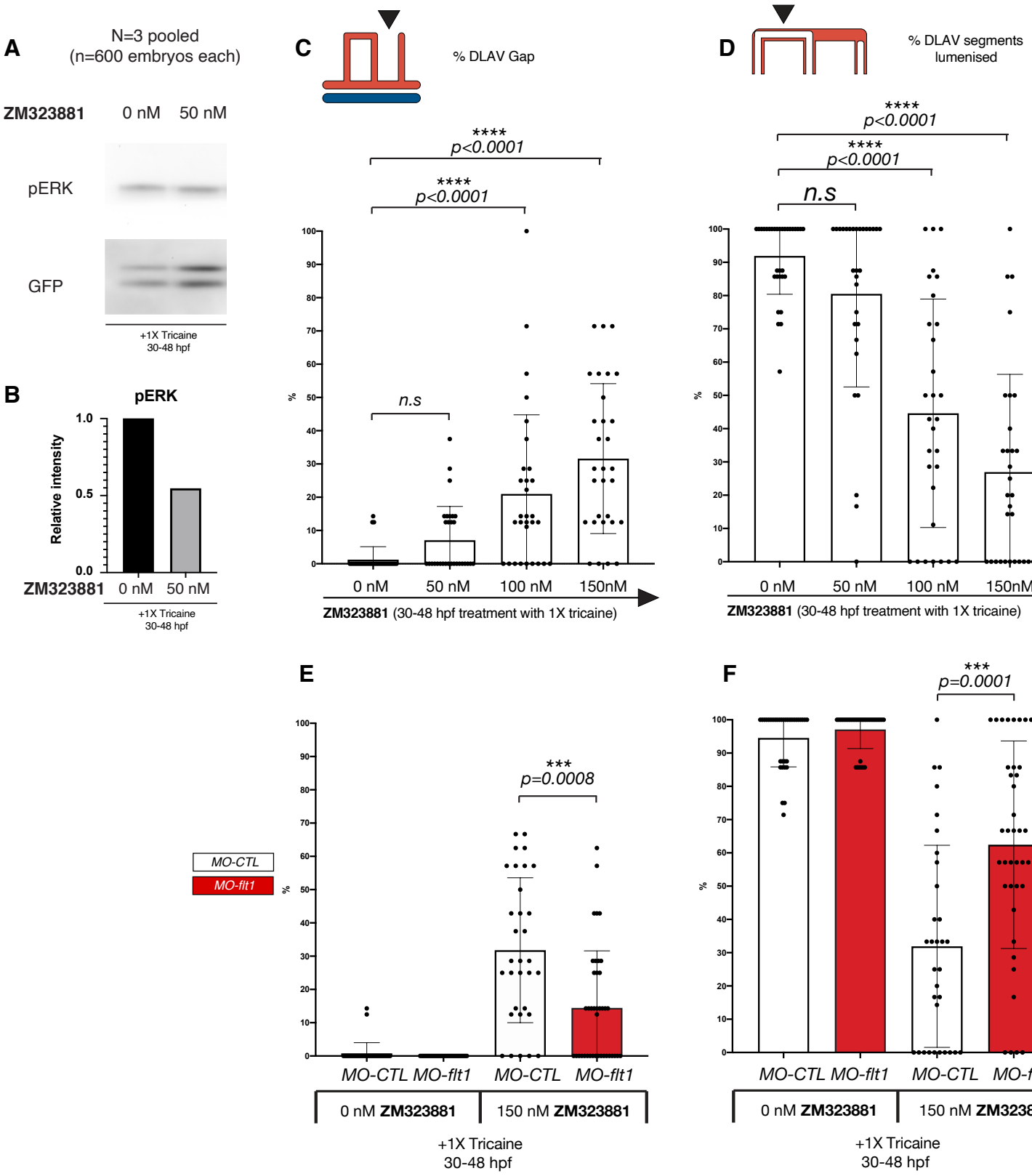

Fig. S4. (A) Representative image of p-ERK and GFP levels in FAC sorted endothelial cells from embryos treated with 1X (0.014%) tricaine from 30 to 48 hpf and 0nM (n=600 embryos – 290637 cells) or 50 nM (n=600 embryos, 300116 cells) ZM323881(N=3 experiments, pooled).

(B) Quantification of p-ERK in FAC sorted endothelial cells from embryos treated with 1X (0.014%) tricaine from 30 to 48 hpf and 0nM (n=600 embryos – 290637 cells) or 50 nM (n=600 embryos, 300116 cells) Expression levels were normalised to GFP levels (N=3 experiments, pooled).

(C) Bilateral quantifications of the percentage of gaps in the DLAV at 48 hpf in WT embryos treated with 1X (0.014%) tricaine and 0 (n=16), 50 (n=15), 100 (n=15) and 150 nM (n=15) ZM32881 from 30 to 48 hpf (N=3). Kruskall-Wallis Anova test.

(D) Bilateral quantifications of the percentage of lumenised segments in the DLAV at 48 hpf in WT embryos treated with 1X (0.014%) tricaine and 0 (n=16), 50 (n=15), 100 (n=15) and 150 nM (n=15) ZM32881 from 30 to 48 hpf (N=3). Kruskall-Wallis Anova test.

(E) Bilateral quantifications of the percentage of gaps in the DLAV at 48 hpf in *MO-CTL* (5 ng) (n=17 (0nM ZM32881), n=16 (150nM ZM32881)) *MO-flt1* (1ng) n=17 (0 nM ZM32881), n=20 (150nM ZM32881)) embryos treated with 1X (0.014%) tricaine and 0 or 50 nM ZM32881 from 30 to 48 hpf (N=4).

(F) Bilateral quantifications of the percentage of lumenized segments in the DLAV at 48 hpf in *MO-CTL* (5 ng) (n=17 (0nM ZM32881), n=16 (150nM ZM32881)) *MO-flt1* (1ng) (n=17 (0 nM ZM32881), n=20 (150nM ZM32881)) embryos treated with 1X (0.014%) tricaine and 0 or 50 nM ZM32881 from 30 to 48 hpf (N=4).

Supplementary Figure 5

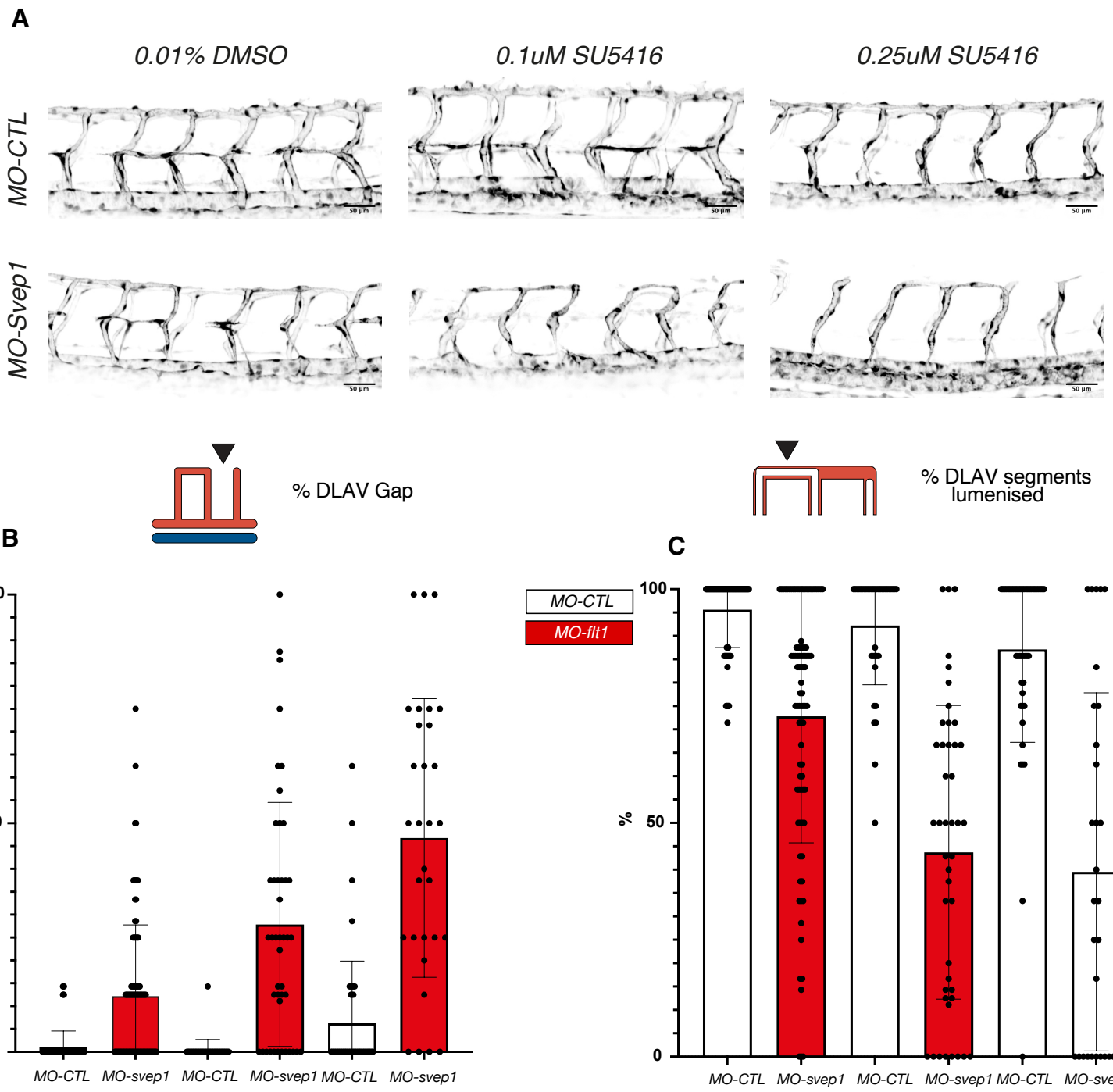

Fig. S5. A) Representative images of *Tg(fli1a:eGFP)^{y1}* embryos at 48 hpf, following treatment with 1X (0.014%) tricaine from 30 hpf, in combination with 0.01%DMSO, 0.1μM SU5416 or 0.25μM SU5416.

B) Bilateral quantifications of the percentage of gaps in the DLAV at 48 hpf in *MO-CTL* (5 ng) (n=80 (0.01% DMSO), n=38 (0.1μM SU5416), n=46 (0.25uM DMSO), n=30 (0.5μM SU5416)) *MO-svep1* (5ng) (n=88 (0.01% DMSO), n=44 (0.1μM SU5416), n=30 (0.25μM DMSO), n=22 (0.5μM SU5416)) embryos treated with 1X (0.014%) tricaine and 0.01% DMSO (N=6) or 0.1 (N=3), 0.25 (N=4), 0.5μM (N=4) SU5416 from 30 to 48 hpf.

C) Bilateral quantifications of the percentage of lumenised segments in the DLAV at 48 hpf in *MO-CTL* (5 ng) (n=80 (0.01% DMSO), n=38 (0.1μM SU5416), n=46 (0.25uM DMSO), n=30 (0.5μM SU5416)) *MO-svep1* (5ng) (n=88 (0.01%DMSO), n=44 (0.1μM SU5416), n=30 (0.25μM DMSO), n=22 (0.5μM SU5416)) embryos treated with 1X (0.014%) tricaine and 0.01% DMSO (N=6) or 0.1 (N=3), 0.25 (N=4), 0.5μM (N=4) SU5416 from 30 to 48 hpf.

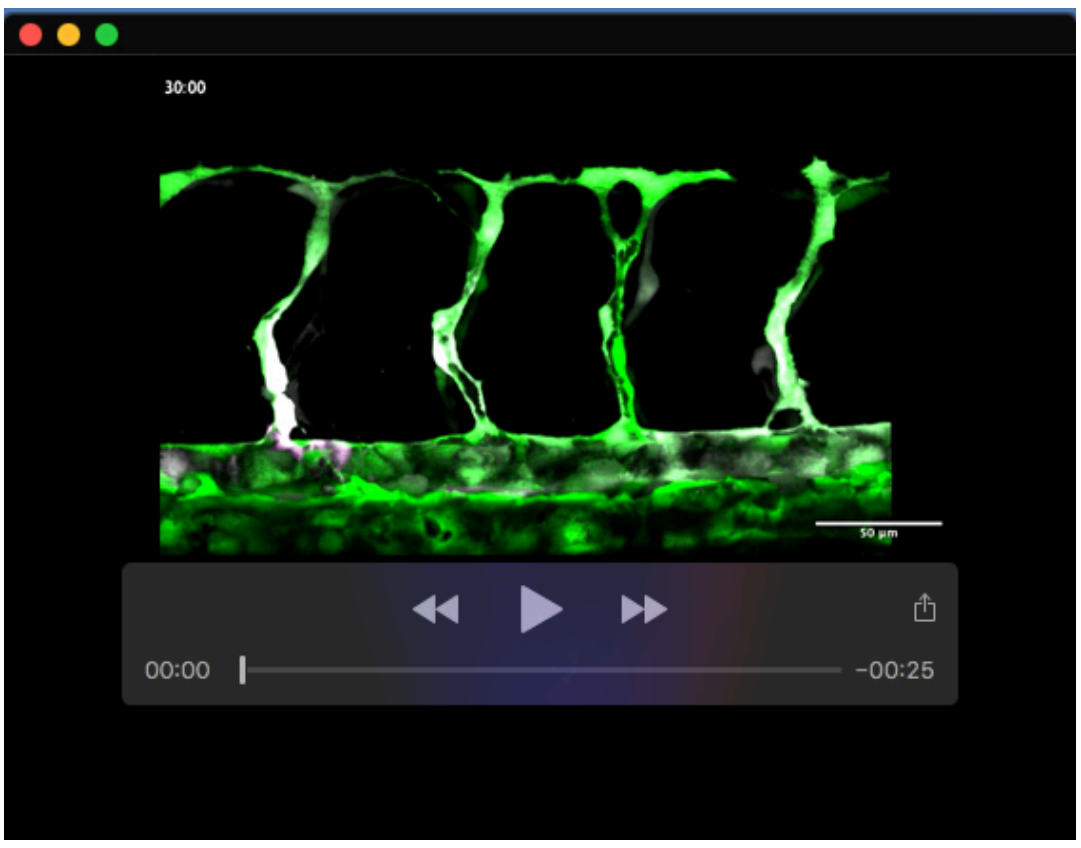

Movie 1. Time lapse movie of *MO-CTL* (5ng) *Tg(-0.8flt1:RFP)^{hu3333}; TgBAC(flt4:Citrine)* embryo treated with 1X (0.014%) tricaine from 30 to 48 hpf. 15-minute interval between frames.

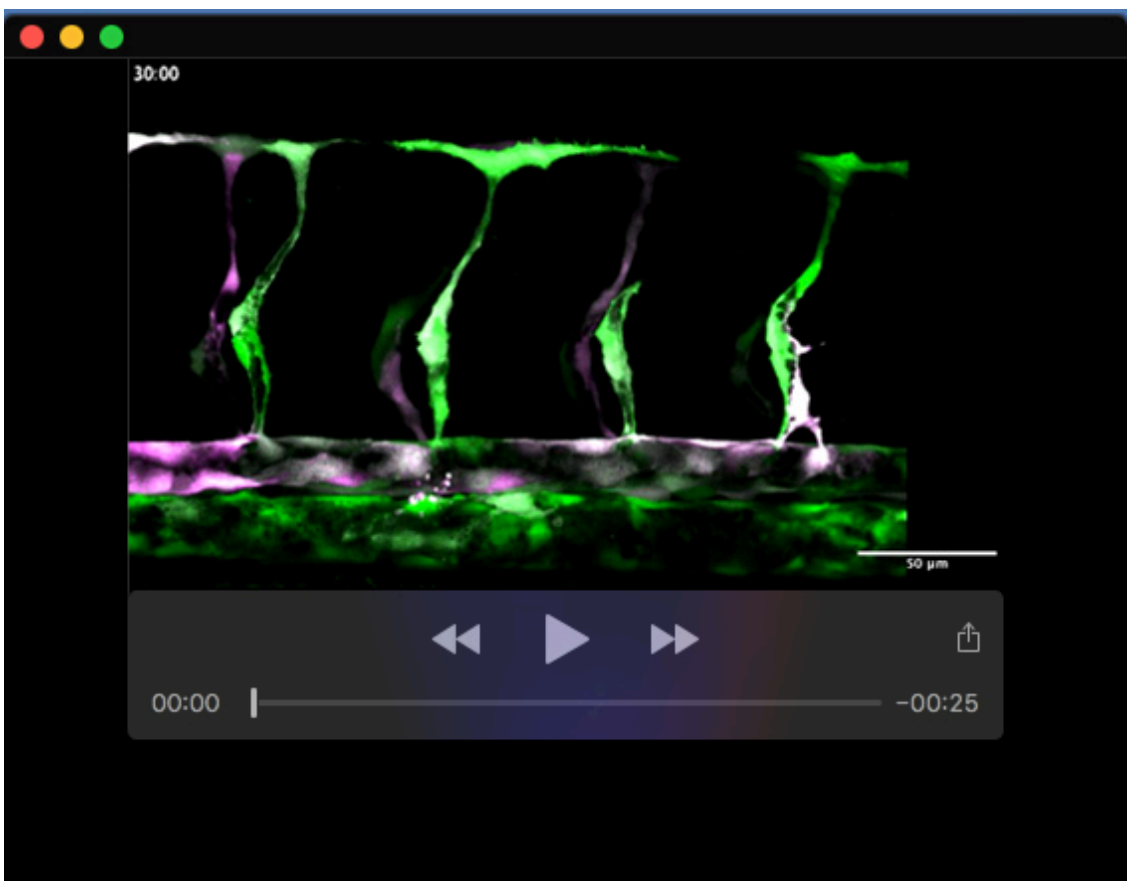

Movie 2. Time lapse movie of *MO-svep1* (5ng) *Tg(-0.8flt1:RFP)^{hu3333}; TgBAC(flt4:Citrine)* embryos treated with 1X (0.014%) tricaine from 30 to 48 hpf. 15-minute interval between frames.